We are IntechOpen, the world's leading publisher of Open Access books Built by scientists, for scientists

6,900
Open access books available

186,000
International authors and editors

200M
Downloads

Our authors are among the

154
Countries delivered to

TOP 1%
most cited scientists

12.2%
Contributors from top 500 universities

CLARIVATE ANALYTICS
BOOK CITATION INDEX
INDEXED

WEB OF SCIENCE™

Selection of our books indexed in the Book Citation Index
in Web of Science™ Core Collection (BKCI)

Interested in publishing with us?
Contact book.department@intechopen.com

Numbers displayed above are based on latest data collected.
For more information visit www.intechopen.com

Biomedical Engineering Professional Trail from Anatomy and Physiology to Medicine and Into Hospital Administration: Towards Higher-Order of Translational Medicine and Patient Care

Dhanjoo N. Ghista

Department of Graduate and Continuing Education,
Framingham State University, Framingham, Massachusetts,
USA

1. Introduction

1.1 Theme

For Biomedical Engineering (BME) to be a professional discipline, we need to address the professional needs of anatomy and physiology, medicine and surgery, hospital performance and management.

The role of BME in Anatomy is to demonstrate how anatomical structures are intrinsically designed as optimal structures. In Physiology, the BME formulation of physiological systems functions can enable us to characterize and differentiate normal systems from dysfunctional and diseased systems. In order to address Medical needs, we need to cater to the functions and disorders of organ systems, such as the heart, lungs, kidneys, and the glucose regulatory system. In Surgery, we can develop the criteria for candidacy for surgery, carry out pre-surgical analysis of optimal surgical approaches, and design surgical technology and implants. In Hospital management, we can develop measures of cost-effectiveness of hospital departments, budget development and allocation.

For BME in Anatomy, we depict how the spinal disc is designed as an intrinsically optimal structure. For BME in Medicine, we formulate the engineering system analyses of Organ system functions and medical tests,

-   in the form of differential equations (DEqs), expressing the response of the organ system in terms of monitored data,
-   in which the parameters of the DEq are selected to be the organ system's intrinsic functional performance features.

The solution of the organ system's governing DEq is then derived, and made to simulate the monitored data, in order to:

-   evaluate the system parameters,
-   and obtain the normal and disease ranges of these parameters.

These parameters can then be combined into a Non-dimensional Physiological Index (NDPI),

-   by which the system can be assessed in terms of just one "number",
-   whose normal and disease ranges can enable effective medical assessment.

Herein, we demonstrate how this methodology [1, 2] is applied to:

- Treadmill test, for evaluating cardiac fitness;
- Lung ventilation modelling, for assessment of status of mechanically ventilated COPD patients;
- Derive a Cardiac Contractility index, which can be determined non-invasively (in terms of auscultatory pressures) and applied to assess left ventricular contractile capacity;
- Glucose Tolerance tests, to detect diabetic patients and borderline patients at risk of becoming diabetic;
- Non-invasive determination of Aortic Pressure profile, systemic resistance and aortic elastance (*Eao*, to characterize the LV systemic load).

Finally, we have also shown the application of this concept and methodology to hospital management. There is a considerable (and hitherto under developed) scope for application of Industrial Engineering discipline for effective hospital administration, in the form of how to determine and allocate hospital budget to optimise the functional performances of all the hospital departments. This leads us to what can be termed as the *Hospital Management System*.

Herein, we have shown how to formulate a performance index (PFI) for ICU. This index divided by the Resource index gives us the cost-effectiveness index (CEI). The Management strategy is to maintain certain acceptable values of both PFI and CEI for all hospital departments, by judicious allocation of staff to the departments. This enables the determination of the Optimal Resource index (RSI) and hospital budget (HOB) to maintain a balance between PFI and CEI for all the hospital departments. This can constitute the basis of Hospital Management.

2. Anatomy: Spine analysed as an intrinsically optimal structure

2.1 Spinal vertebral body (an intrinsically efficient load-bearer)

The spinal vertebral body (VB) geometry resembles a hyperboloid (HP) shell (fig 2) which is loaded by compressive and torsional loadings, portrayed in fig 1 as resolved into component forces along its generators.
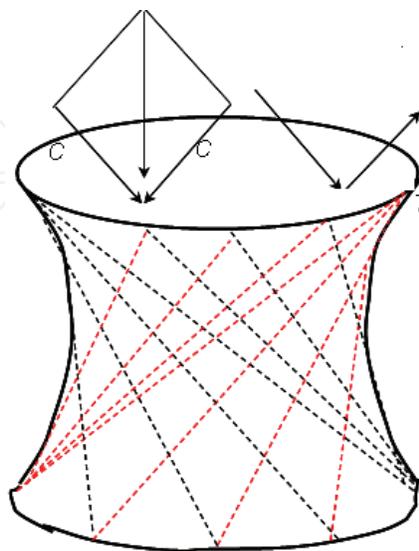

Fig. 1. Vertebral body, a hyperboloid (HP) shell formed of 2 sets of generators [3].

Stress analysis of the VB under Axial Compression [3]:
We now analyse for stresses in the HP shell (generators) due to a vertical compressive force
P, as shown in figures 3 and 4.Assume that there are two sets of '*n*' number of straight bars
placed at equal spacing of ($2\pi a/n$) measured at the waist circle, to constitute the HP surface,
as shown in figure 3 (right). Due to the axi-symmetric nature of the vertical load, no shear
stresses are incurred in the shell, i.e. $\sigma_{\phi\theta}=0$, as in figure 3 (left). We then delineate a segment
of the HP shell, and consider its force equilibrium (as illustrated in figure 4), to obtain the
expressions for stresses N_ϕ and N_θ as depicted in figure 4.

Straight-line (generator)
tangent to the waist circle
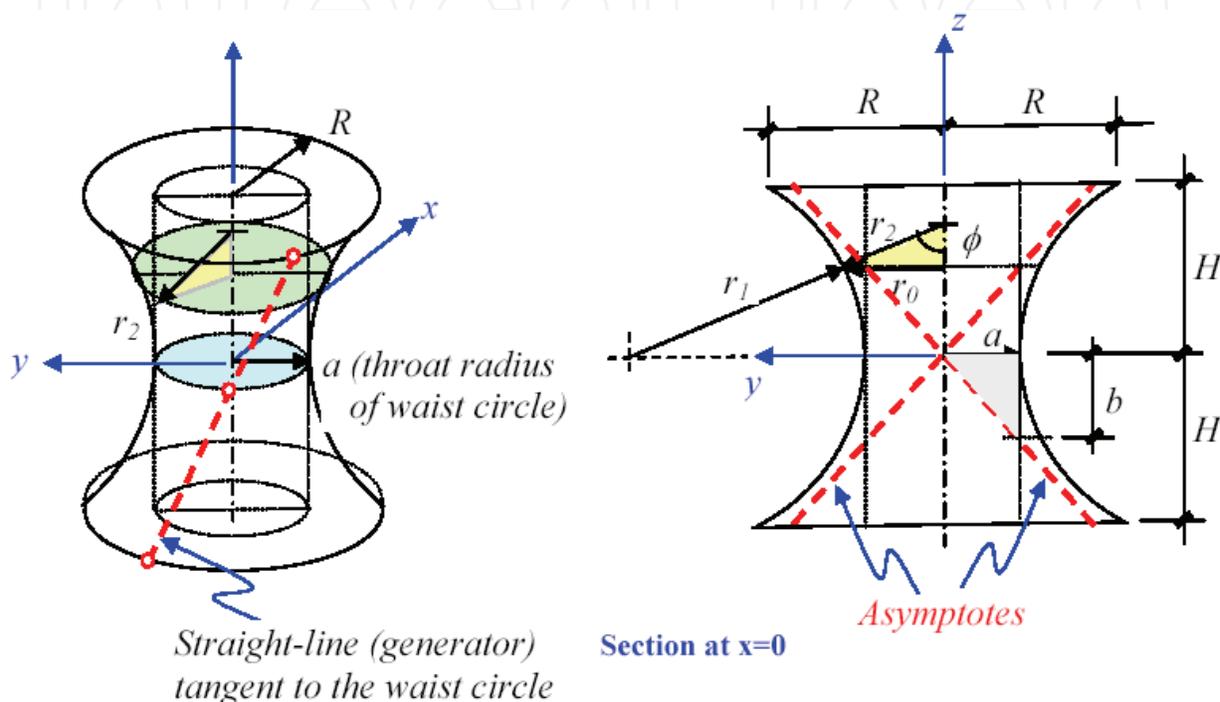
Section at x=0

r$_1$: radius of curvature of meridian

r$_2$: slanted radius of horizontal section
having radius *r$_o$*

Kinematic Relationship:

$$r_o = r_2 \, (sin\phi)$$

$$r_1 = -\left(\frac{b^2}{a^4}\right) r_2^3$$

Equation of HP curves:

$$\frac{x^2 + y^2}{a^2} - \frac{z^2}{b^2} = 1$$

$$At \ x = 0, \quad \frac{y^2}{a^2} - \frac{z^2}{b^2} = 1$$

Equation of asymptotes:

$$z = \pm\left(\frac{b}{a}\right) y$$

Fig. 2. Geometry of a Hyperboloid (HP) shell. In the figure z = b, and y = a. We define tan
β = a/b [3].
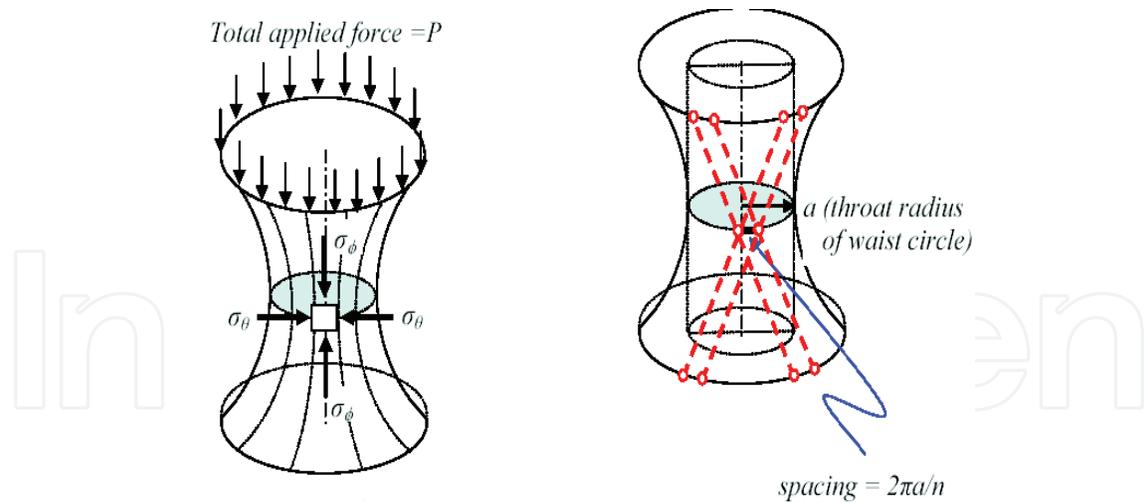
Fig. 3. Stress Analysis for Vertical Loading: Stresses at the waist section of the VB HP Shell: (a) stress components (b) equivalent straight bars aligned with the generators) placed at equal spacing to take up the stresses. In fig 3 (left) due to axi-symmetric vertical load, no shear stresses are incurred in the shell, i.e. $\sigma_{\phi\theta}=0$. In fig 3 (b), there are 2 sets of 'n' number of straight bars placed at equal spacing of $(2\pi a/n)$ measured at the waist circle, to constitute the generators of the HP surface [3].

Equilibrium of Forces on a Shell Segment under Vertical load P:

At the waist ($r_o = a$),

$$N_\phi = \frac{P}{2\pi a}, \text{ compressive}$$

Now since, $\dfrac{N_\phi}{r_1} - \dfrac{N_\theta}{r_2} = p_r$

Hence,

$$N_\theta = \left(\frac{a^2}{b^2}\right)\frac{P}{2\pi a} = \frac{P\tan^2\beta}{2\pi a}$$
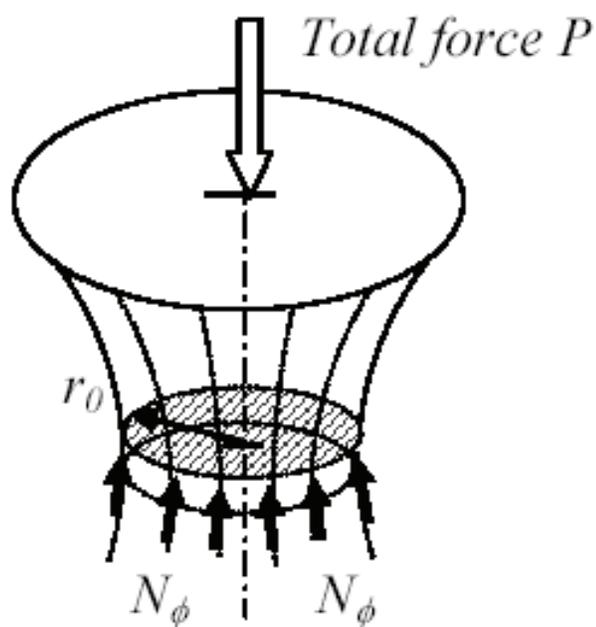
Fig. 4. Equilibrium of Forces on a Shell Segment: Analysis for stresses N_ϕ and N_θ due to the vertical force P [3,2].

Then based on the analysis in Fig 5, we obtain the expression for the equivalent resultant compressive forces C in the fibre-generators of the VB HP shell. Thus it is seen that the total axial loading is transmitted into the HP-shell's straight generators as compressive forces. It is to be noted that the value of C is independent of dimensions R and a.
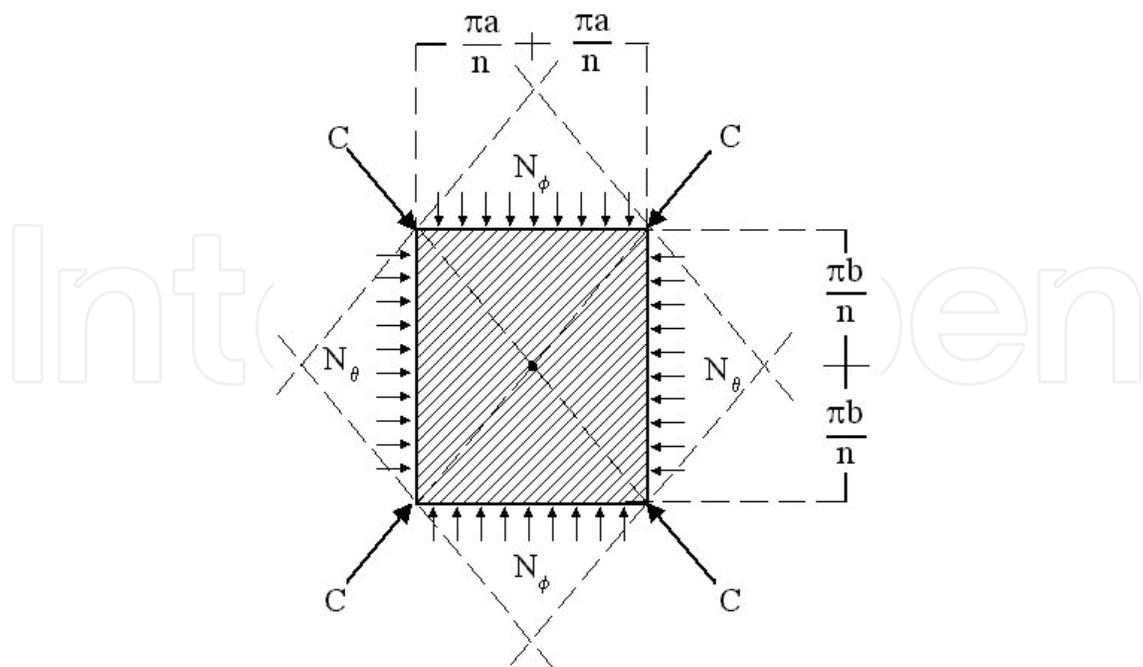
$$N_\phi = P / 2\pi a \text{ and}$$

$$N_\theta = (a^2 / b^2)P / 2\pi a$$

result in

$$C^2 = \left(N_\phi \frac{\pi a}{n} \right)^2 + \left(N_\phi \frac{\pi b}{n} \right)^2$$

$$C = \frac{P}{2nb}\sqrt{b^2 + a^2}$$

$$= \frac{P}{2n\cos\theta} = \frac{P(H^2 + a^2 - a^2)^{1/2}}{2nH}$$

Fig. 5. Equivalent compressive force C in the generators (corresponding to the stress-resultants acting on the shell element) equilibrating the applied axial loading [3,2].

It can be noted that the value of C is independent of dimensions R and a.

Stress analysis under Torsional loading [3]:

Next, we analyse the compressive and tensile forces in the HP shell generators when the VB is subjected to pure torsion (*T*).In this case (referring to **fig. 6)**, the normal stress resultants are zero, and we and only have the shear stress-resultant , as given by

$$N_\phi = N_\theta = 0 \qquad \text{and} \quad N_{\phi\theta} = \tau \text{t}$$

The equilibrium of a segment of the shell at a horizontal section at the waist circle (depicted in **figure** 6 **a**) gives the shear stress-resultant as follows:

$$[(\tau \cdot t)(2\pi a)]a = T \text{ , i.e., } N_{\phi\theta} = \frac{T}{2\pi a^2}$$

Stress Analysis for Torsional Loading M

For equilibrium,
$$(2\pi a)(\tau \cdot t)a = M$$
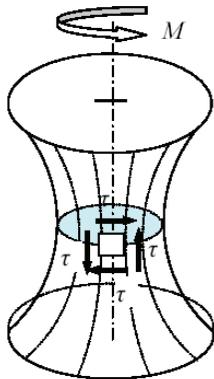
$$\tau = \frac{M}{2\pi a^2 t}$$

$$N_{\phi\theta} = \frac{M}{2\pi a^2}$$

Equilibrium of a shell segment under torsion (M) and shear stresses (τ) (or shear stress-resultant $N_{\phi\theta}$)
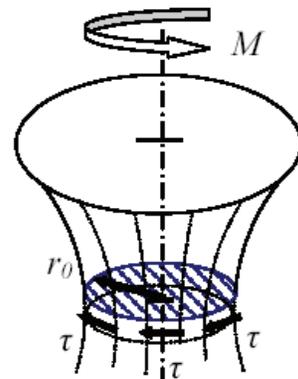
Stresses in the HP shell element ($\sigma_\phi = \sigma_\theta = 0$ and $\sigma_{\phi\theta} = \tau$) due to torsion M acting on the VB

Fig. 6. Stress analysis of the vertebral body under torsional loading [3].

Now, we consider an element at the waist circle as shown in **figure** 7. The equivalent compressive force (F_{cT}) and tensile force (F_{tT}), in the directions aligned to their respective set of shell generators, are given by

$$F_{cT}^2 = F_{tT}^2 = \left(N_{\phi\theta}\frac{\pi a}{n}\right)^2 + \left(N_{\phi\theta}\frac{\pi b}{n}\right)^2$$

or,
$$\left|F_{cT}\right| = \left|F_{tT}\right| = \frac{T}{2na\sin\beta}$$

wherein F_{cT} and F_{tT} are depicted as c and T respectively in figure 7.

$$= \frac{M(a^2 + a^2\cot^2\theta)^{1/2}}{2na^2}$$

$$= \frac{M}{2na\sin\theta}\left|T\,or\,C\right|$$

$$= \frac{M\cos ec\,\theta}{2na}$$
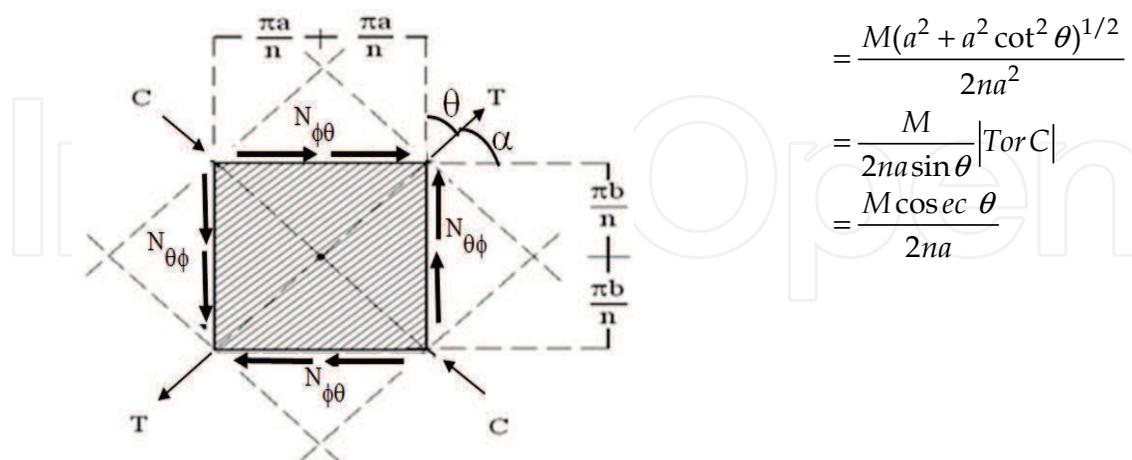
Fig. 7. Analysis of equilibrium of a shell element comprising of two intersecting generators: Expressions for tensile forces T and compressive forces C in the generators, indicate that torsion loading is also transmitted as axial compressive and tensile forces through the generators of the VB, which makes it a naturally optimum (high-strength and light-weight) structure [3].

Thus, a torsional loading on the VB HP shell is taken up by one set of generators being in compression and the other set of generators being in tension.

Equilibrium of a Shell Element Comprising of Two Intersecting Generators: The equivalent compressive forces (*C*) and tensile forces (*T*); in the shell generators (required to equilibrate the applied load), are given by:

$$|T| = |C| = \sqrt{\left(\tau \cdot t\left(\frac{\pi a}{n}\right)\right)^2 + \left(\tau \cdot t\left(\frac{\pi b}{n}\right)\right)^2} = \tau \cdot t\left(\frac{\pi}{n}\right)\sqrt{a^2 + b^2} = \frac{M(a^2 + b^2)^{1/2}}{2na^2}$$

2.2 Spinal disc optimal design (to bear loading with minimal deformation and maximal flexibility)

Fig 8 illustrates how the mechanism of how the spinal disc bears compression without bulging. It is seen that the nucleus pulposus plays the key role in this mechanism, as will be explained further in this section. Hence the absence of it in a denucleated disc causes the disc to bulge.
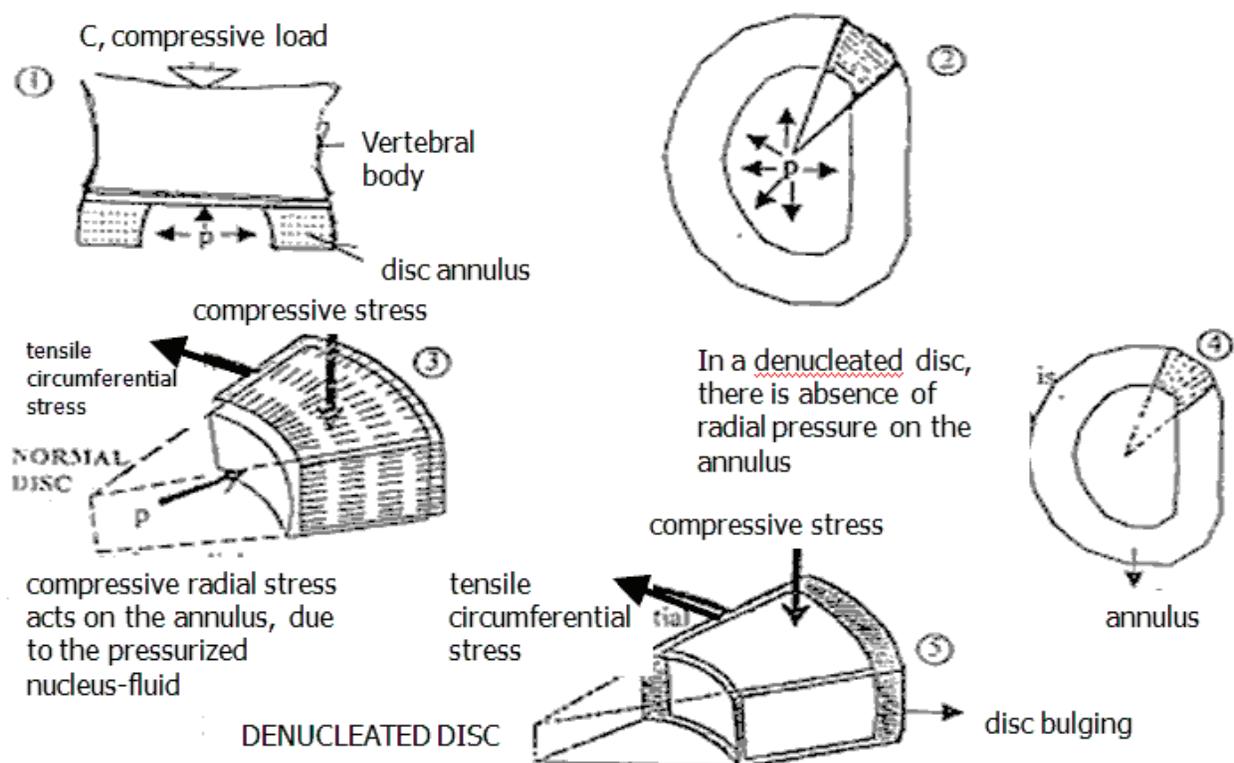

Fig. 8. Mechanism of how the spinal disc bears compression without bulging.

Fig 9 displays the geometry and the deformation variables of the spinal disc. We now present the elasticity analysis of the disc to first obtain the radial, circumferential and axial stresses in terms of the disc deformations and annulus modulus *E*[4].

We next carry out the stress analysis of the disc under vertical loading *P* (fig 10), to obtain the expressions (equations 10) for the stresses in the disc annulus in terms of the load *P* , pressure p in the nucleus-pulposus, and the disc dimensions (a and b) [4].

We then derive the expressions for the disc axial and radial deformations δ_u and δ_h in terms of nucleus pulposus pressure *p*, the annulus modulus *E* and the disc dimensions, as given

by equations (17) and (18). Now the annulus modulus E is a function of the stress in the annulus (k being the constitutive proportionality constant), and hence of the pressure p and the disc dimensions, as shown by equation (21). As a result of this relationship, we finally show that the disc deformations are only functions of k and the disc dimensions. This implies that irrespective of the increase in the value of load P, the disc deformations remain constant, and only depend on the constitutive property parameter k. This is the novelty of the intrinsic design of the spinal disc!
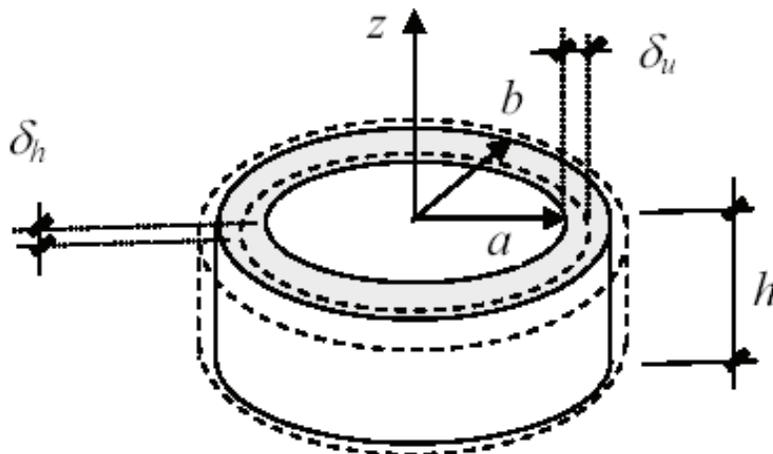

Fig. 9. Geometry and Deformation Variables of the Spinal Disc [4].

ANALYSIS
The equilibrium equation is:

$$\sigma_r - \sigma_\theta + r\frac{d\theta_r}{dr} = 0 \tag{1}$$

Strain-displacement relations:
$$\in_r = \frac{du}{dr}, \in_\theta = \frac{u}{r}, \tag{2}$$

Constitutive relations:

$$\sigma_r = E\in_r = E\frac{du}{dr}, \ \sigma_\theta = E\in_\theta = E\frac{u}{r} \tag{3}$$

Substituting eqn (3) into eqn (1), we have:

$$\frac{d^2u}{dr^2} + \frac{1}{r}\frac{du}{dr} - \frac{u}{r^2} = 0, \ u = Ar + \frac{B}{r} \tag{4}$$

Because of the incompressible nucleus pulposus fluid inside:

$$\pi a^2 h = \pi(a + \delta_u)^2(h - \delta_h) \tag{5}$$

the (radial and axial) deformations δ_u and δ_h are related as:

$$\delta_u = \frac{\pi a^2 \delta_h}{2\pi a h} = \left(\frac{a}{2h}\right)\delta_h \tag{6}$$

Now, we designate:

$$u\big|_{r=a} = \delta_u, \sigma_r\big|_{r=b} = 0 \tag{7}$$

Substituting eqn (7) into eqns (3 & 4), we get

$$Aa + \frac{B}{a} = \delta_u$$

$$E\left[A - \frac{B}{b^2}\right] = 0 \tag{8}$$

So that

$$A = \frac{a\delta_u}{a^2 + b^2}, \quad B = \frac{a\delta_u.b^2}{a^2 + b^2} \quad \text{in the 'u' function} \tag{9}$$

Then, substituting A and B into eqns (4 & 3), we obtain:

- for the radial stress, $\quad \sigma_r = \dfrac{Ea\left(r^2 - b^2\right)\delta u}{(a^2 + b^2)r^2} = \dfrac{a^2\left(r^2 - b^2\right)}{2h(a^2 + b^2)r^2}E\delta h \tag{10-a}$

- for the circumferential stress, $\quad \sigma_\theta = \dfrac{Ea\left(r^2 + b^2\right)\delta u}{(a^2 + b^2)r} = \dfrac{a^2\left(r^2 + b^2\right)}{2h(a^2 + b^2)r}E\delta h \tag{10-b}$

- for the axial stress $\quad \sigma_z = E\in_z = E\dfrac{\delta_h}{h} \quad \delta u = \left(\dfrac{a}{2h}\right)\delta h \tag{10-c}$

Once σ_z is evaluated, δ_h will become known (from eqn. 10-c) and subsequently σ_r, σ_θ (from eqns 10-a & 10-b) and δ_u (from eqn 10-c).

Stress Analysis for Vertical Loading [4]:

For a vertically applied force P,

$$P = \left(\pi a^2\right)\sigma_f + \pi(b^2 - a^2)\sigma_z \tag{11}$$

where σ_f is the hydrostatic pressure in the NP fluid, and σ_z the axial stresses in the annulus. Because the disc height (h) is small, $\sigma_f \approx constant$, and hence

$$\sigma_f = -\sigma_r\big|_{r=a} = p \tag{12}$$

Then, based on eqns (12, 10-a & 10-c), we obtain

$$\sigma_f = -\frac{\left(a^2 - b^2\right)}{2h\left(a^2 + b^2\right)}E\delta h = \frac{\left(b^2 - a^2\right)}{2h\left(a^2 + b^2\right)}E\left(\frac{\delta_h}{h}\right), \text{ or } \sigma_f = \frac{(b^2 - a^2)}{2(a^2 + b^2)}\sigma_z = p \tag{13}$$

Note:
σ_f : induced fluid pressure
σ_z : compressive stress induced in the annulus
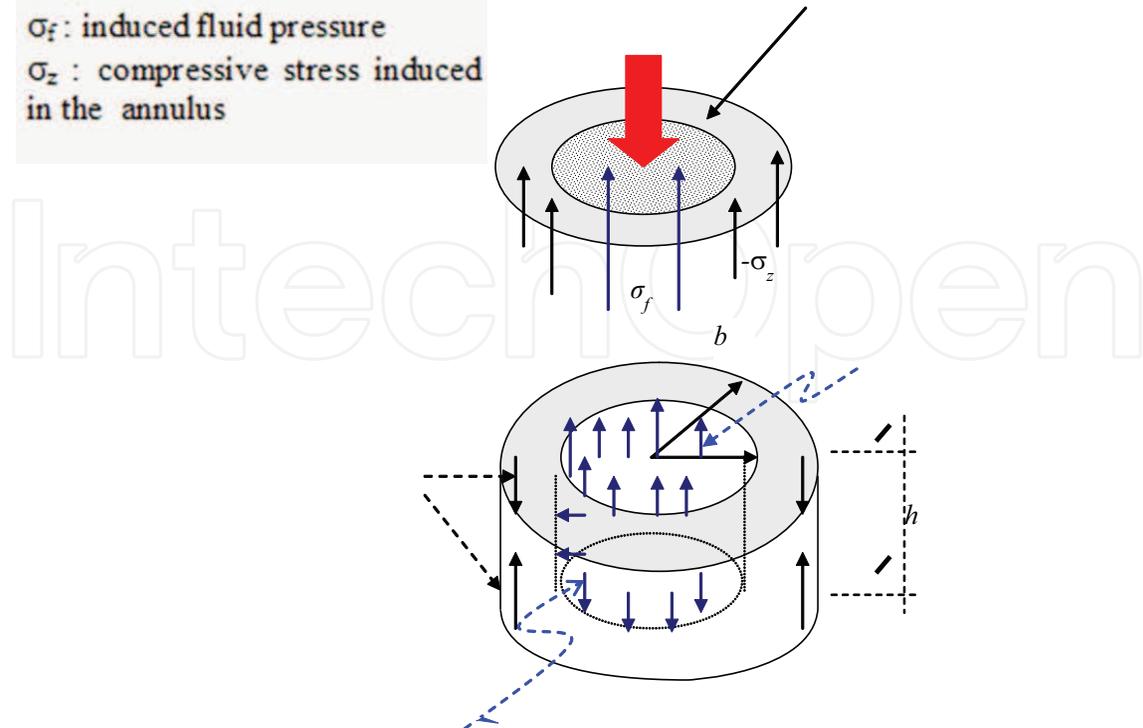
Normal stresses σ_f & σ_z equilibrating the applied force P

Fig. 10. Induced Stresses in the disc annulus and Pressure p in the nucleus-pulposus in response to the load P [4].

Substituting

$$\sigma_f = \frac{\left(b^2 - a^2\right)}{2\left(a^2 + b^2\right)}, \quad \sigma_z = p, \ \sigma_z = E\frac{\delta h}{h} = 2E\frac{\delta u}{a}$$

Into

$$P = (\pi a^2)\sigma_f + \pi(b^2 - a^2)\sigma_z$$

We get:

$$\delta_h = \frac{h\sigma_z}{E} = \frac{h}{E} \ \frac{P}{\pi(b^2 - a^2)}\left[\frac{2(a^2 + b^2)}{3a^2 + 2b^2}\right] \tag{14}$$

$$\delta_u = \frac{a}{2h}\delta_h = \frac{a}{2E} \ \frac{P}{\pi(b^2 - a^2)}\left[\frac{2(a^2 + b^2)}{3a^2 + 2b^2}\right] \tag{15}$$

Nucleus-pulposus fluid pressure, $$p = \frac{P}{\pi(3a^2 + 2b^2)} \tag{16}$$

$$\sigma_z = \frac{2p(a^2 + b^2)}{(b^2 - a^2)} = \frac{2P(a^2 + b^2)}{\pi(b^2 - a^2)(3a^2 + 2b^2)} \tag{16-a}$$

$$\delta_h = \frac{h\sigma_z}{E} = \frac{h}{E} \quad \frac{P}{\pi(b^2 - a^2)}\left[\frac{2(a^2 + b^2)}{3a^2 + 2b^2}\right]$$

Stress in the Annulus

From,

$$\sigma_\theta = \frac{Ea\left(r^2 + b^2\right)\delta_u}{(a^2 + b^2)r} = \frac{a^2\left(r^2 + b^2\right)}{2h(a^2 + b^2)r}E\delta_h$$

We get :

$$\frac{a^2\left(r^2 + b^2\right)P}{\pi r^2(b^2 - a^2)(3a^2 + 2b^2)} = \frac{pa^2\left(r^2 + b^2\right)}{r^2(b^2 - a^2)},\qquad (17)$$

$$\sigma_\theta(\text{r} = \text{a}) = \frac{p\left(a^2 + b^2\right)}{(b^2 - a^2)},\ \text{ in the annulus}\qquad (18)$$

wherein, $p = \dfrac{P}{\pi\left(3a^2 + 2b^2\right)}$, pressure in nucleus-pulposus fluid

The disc deformations have been obtained as:

Axial deformation,

$$\delta_h = \frac{2ph(a^2 + b^2)}{E_c(b^2 - a^2)}\qquad (19)$$

Radial deformation

$$\delta_u = \frac{pa(a^2 + b^2)}{E_c(b^2 - a^2)}\qquad (20)$$

wherein $E_c = E - E_o = k\sigma$.

$$\therefore E_c = k\sigma_\theta(r = a) = kp\frac{(a^2 + b^2)}{(b^2 - a^2)}\qquad (21)$$

Now, as the magnitude of the load P increases, the pressure p in nucleus-pulposus fluid also increases. Then, as p increases, so does the modulus E_c according to eqn (21)

$$\therefore \frac{p}{E_c} = \frac{\left(b^2 - a^2\right)}{k\left(a^2 + b^2\right)} = \text{constant}\qquad (23)$$

$$\delta_h = \frac{2ph(a^2 + b^2)}{E_c(b^2 - a^2)} = \frac{2h}{k}\text{ , a constant, and } \delta_u = \frac{pa(a^2 + b^2)}{E_c(b^2 - a^2)} = \frac{2a}{k}\text{ , a constant}$$

This means that, irrespective of increase in the value of load P, the disc deformations δ_u and δ_h remain constant, and only depend on the constitutive property parameter k. This is the novelty of the intrinsic design of the spinal disc!

3. Physiology: Mechanism of left ventricle twisting and pressure increase during isovolumic contraction (due to the contraction of the myocardial fibres)

Introduction and objective: The left ventricular (LV) myocardial wall is made up of helically oriented fibers. As the bioelectrical wave propagates along these fibers, it causes concomitant contraction wave propagation. Our LV cylindrical model is illustrated in figure 11. The contraction of the helical oriented myocardial fibers causes active twisting and compression of the LV (as illustrated in fig 11), thereby compressing the blood fluid contained in it. Then due to the very high bulk modulus of blood, this fluid compression results in substantial pressure increase in the LV cavity.

Herein we simulate this phenomenon of LV isovolumic contraction, which causes the intra-LV pressure to rise so rapidly during 0.02-0.06 seconds of isovolumic contraction. Our objective is to determine how the pressure generated during isovolumic contraction, due to by active torsion (with LV twisting) and compression (with LV shortening) caused by the contractile stress in the helically wound myocardial fibers [5].
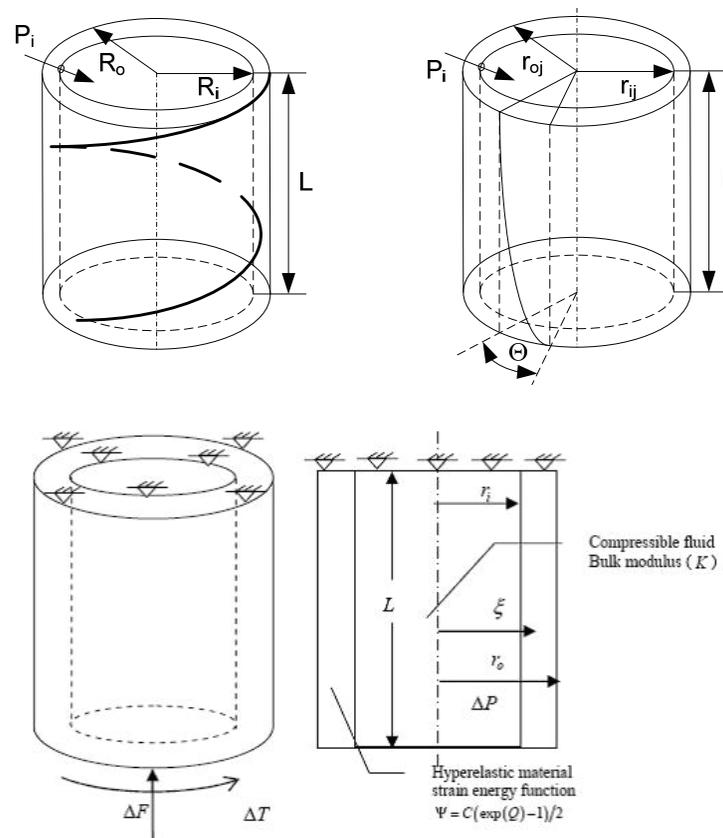

Fig. 11. Top: Fiber orientation and twisting model of the left ventricle (LV). Bottom: The fluid-filled LV cylindrical shell model: (i) geometry (ii) material property, and (iii) equivalent compression ΔF and ΔT associated with its internal stress state due to internal pressure rise within it.

Concept: In order to simulate the left ventricle deformation during isovolumic contraction, we have modeled it as a pressurized fluid-filled thick-walled cylindrical shell supported by the aorta along its upper edge. The LV cylindrical model consists of an incompressible hyperelastic material with an exponential form of the strain energy function ψ.

The contraction of the myocardial fibers causes active twisting and compression of the left ventricle, thereby compressing the blood fluid contained in it. Then, due to the very high bulk modulus of blood, this compression results in pressure increase in the ventricular cavity. Hence, we simulate this phenomenon by applying and determining equivalent active torque and compression to the LV-cylindrical model incrementally (as ΔF and ΔT), so as to raise the LV pressure by the monitored amounts.

Modeling approach:

We monitor LV pressure (p), LV volume (V), myocardial volume (V_M), and wall thickness (h) at time intervals during isovolumic contraction. From the monitored V, V_M, and h, we determine the LV model radius R and length L and the wall thickness h. We also monitor LV twist angle ϕ.

We then invoke blood compressibility to determine ΔV at subsequent instants , as $\Delta V = (\Delta p/K) V$, where Δp is the monitored incremental pressure and K is the bulk modulus of blood. From the volume strain $\Delta V/V$, we then determine the model length and radius strains $\Delta I/L$ and $\Delta r/R$, and hence the LV dimensions with respect to LV dimensions at the start of isovolumic contraction. This enables us to determine the stretches (strains) (λ_z, λ_r, λ_θ and γ), and thereafter the Lagrange strain tensor components (E_{rr}, $E_{\theta\theta}$, E_{zz}, $E_{\theta z}$) in terms of these stretches and the hydrostatic pressure.

Then, we express the LV wall stresses in terms of the strain energy density function Ψ, of the Lagrange strain tensor components in cylindrical coordinates and the material constitutive parameters (b_i), in which (i) the stretches (λ_z, λ_r, λ_θ and γ) have been calculated and are known, (ii) the hydrostatic pressure and the constitutive parameters b_i (i = 1, 2, . . . , 9) are the unknowns.

So now, we substitute the stress expressions σ_{rr} and $\sigma_{\theta\theta}$ into the boundary conditions equations (of equilibrium between the internal pressure and the wall stresses σ_{rr} and $\sigma_{\theta\theta}$, and between the internal pressure and wall stress σ_{zz}), and determine the best values of the constitutive parameters (b_i) and the hydrostatic pressure to satisfy these equations.

We then go back, and determine the stress expressions. We utilize the stress expressions for σ_{zz} and $\sigma_{\theta z}$, to determine the generated values of torsion (ΔT) and axial compression (ΔF),due to the contraction of the helically wound myocardial fibres.

Finally, we determine the principal stresses and principal angle along the radial coordinate of the LV wall thickness, from which we can interpret the fibre orientations, which can be related to the LV contractility index.

This procedure is carried out at three instants of time from the start of isovolumic contraction, and at 0.02 s, 0.04 s, 0.06 s into the isovolumic contraction phase. Hence, from the monitored LV Δp and computed ΔV at these three instants (with respect to the pressure and volume at t = 0 at the start of isovolumic contraction phase, we determine (i) the time variation of the internally generated torque and axial compression during the isovolumic contraction phase (fig 12), as well as (ii) the time variations of the principal (tensile) stress and the principal angle (taken to be equivalent to the fiber angle) during the isovolumic contraction phase (fig 13).

Model Kinematics:

We model the LV as an incompressible thick-walled cylindrical shell subject to active torsion torque and compression as illustrated in fig 11. The upper end of the LV model is

constrained in the long-axial direction to represent the suspension of the left ventricle by the aorta at the base. Now, considering the LV at end-diastole to be in the unloaded reference configuration, the cylindrical model in its undeformed state is represented geometrically in terms of cylindrical coordinates (R, Θ, Z) by

$$R_i \leq R \leq R_o, \ \ 0 \leq \Theta \leq 2\pi, \ \ 0 \leq Z \leq L \tag{1}$$

where R_i, R_o and L denote the inner and outer radii, and the length of the undeformed cylinder, respectively.

In terms of cylindrical polar coordinates (r, θ, z), the geometry of the deformed LV configuration (with respect to its undeformed state at the previous instant) is given by:

$$r_i \leq r \leq r_o, \ \ 0 \leq \theta \leq 2\pi, \ \ 0 \leq z \leq l \tag{2}$$

where r_i, r_o and l denote the inner and outer radii, and the length of the deformed cylinder, respectively.

We further consider the incompressible LV model in its reference state to be subjected to twisting, radial and axial deformations in the radial and long-axis directions during isovolumic contraction, such that (also based on incompressibility criterion), the deformations of incompressible LV cylindrical shell can be expressed as

$$r = \sqrt{\frac{R^2 - R_i^2}{\lambda_z} + r_i^2} \ , \ \ \theta = \Theta + Z\frac{\phi}{L}, \ z = \lambda_z Z \tag{3}$$

where λ_z is the constant axial stretch, r_i is the inner radius in the deformed configuration and ϕ is the measured angle of twist at the apex of the LV (relative to the base). It can be seen that the twist angle (θ) and the axial deformation (z) are zero at the upper end of the LV.

Model Dimensions:

At any instant (t), the geometrical parameters (or dimensions) of the LV cylindrical model (instantaneous radius R and length L, as defined in fig 11) can be determined in terms of the monitored LV volume (V), myocardial volume (V_M) and wall thickness (h), as follows:

$$R_i = \frac{2Vh / V_M + \sqrt{\left(2Vh / V_M\right)^2 + 4Vh^2 / V_M}}{2} \tag{4-a}$$

$$L = V / \pi R_i^2 \tag{4-b}$$

Then, $$R_o = R_i + h. \tag{4-c}$$

These equations will be employed to determine the LV dimensions at the start of isovolumic contraction phase (t = 0). The determination of the dimensions of the deformed LV (due to contraction of the myocardial fibers) at the subsequent instants of the isovolumic contraction phase is indicated in the next subsection. We also utilize the information on the LV twist angle (ϕ) during the isovolumic phase, from MRI myocardial tagging. From this information, we can determine the stretches (λ_z, λ_r, λ_θ and γ).

Theoretical Analysis:

The strain energy density function suitable for the myocardium material, is given by:

$$\psi = C(\exp(Q) - 1)/2 \tag{5}$$

wherein Q is a quadratic function of the 3 principal strain-components (to describe 3-d transverse isotropy) in the cylindrical coordinate system, given by:

$$Q = b_1 E_{\theta\theta}^2 + b_2 E_{ZZ}^2 + b_3 E_{RR}^2 + 2b_4 E_{\theta\theta} E_{ZZ} + 2b_5 E_{RR} E_{ZZ}$$
$$+ 2b_6 E_{\theta\theta} E_{RR} + 2b_7 E_{\theta Z}^2 + 2b_8 E_{RZ}^2 + 2b_9 E_{\theta R}^2 \tag{6}$$

wherein b_i are non-dimensional material parameters, and E_{ij} are the components of the modified Green-Lagrange strain tensor in cylindrical coordinates (R, Θ, Z). In order to reduce the mathematical complexity of the problem, we assume negligible shear during isovolumic contraction. Thus E_{RZ} and $E_{\theta R}$ in equation (6) and their corresponding stress components (σ_{RZ} and $\sigma_{\theta R}$) are neglected.

The stress equilibrium equation (in the cylindrical coordinate system) is given by the following equation:

$$\frac{d\sigma_{rr}}{dr} + \frac{(\sigma_{rr} - \sigma_{\theta\theta})}{r} = 0 \tag{7}$$

The boundary conditions on the outer and inner surfaces of the LV cylindrical model are given by

$$\sigma_{rr}(r = r_o) = 0 \,\text{,}\, \sigma_{rr}(r = r_i) = -p \tag{8}$$

where p is the LV pressure acting on the inner surface of the LV model; we employ incremental pressure Δp with respect to the LV pressure at t = 0, the start of isovolumic contraction.

By integrating eq (7), the Cauchy radial stress σ_{rr} is given by:

$$\sigma_{rr}(\xi) = \int_\xi^{r_o} (\sigma_{rr} - \sigma_{\theta\theta}) \frac{dr}{r}, \qquad r_i \le \xi \le r_o \tag{9}$$

There from, the boundary condition eq (8) of the internal pressure p = -σ$_{rr}$ (r=r$_i$) is obtained (by substituting equation 9 into the boundary condition 8), in the form:

$$p_i = -\int_{r_i}^{r_o} (\sigma_{rr} - \sigma_{\theta\theta}) \frac{dr}{r}, \tag{10}$$

Since the valves are closed during isovolumic contraction, we impose another set of boundary conditions (at both the top and bottom of the internal LV surface), giving:

$$\sigma_{zz} \pi \left(r_o^2 - r_i^2 \right) = p \left(\pi r_i^2 \right) \tag{11}$$

where σ_{ZZ} denotes the axial component of the Cauchy stresses. In the analysis, we will employ Δp with respect to the pressure at t = 0, at the start of isovolumic contraction.

The blood in the left cavity is assumed compressible, and the change in cavity volume (ΔV) due to the monitored incremental pressure (Δp), is given by

$$\Delta V = \Delta p / K; \qquad K = 2.0 \times 10^9 pa \tag{12}$$

where K is the bulk modulus of blood.

Analysis and computational procedure:

The following analysis is carried out at the three time instants t (or j) = 0.02 secs, 0.04 secs and 0.06 secs (from the start t = 0 of the isovolumic contraction phase, from the monitored Δp and computed ΔV (eq 12) at the three time instants with respect to p and V at t = 0 (the start of isovolumic contraction phase).

1. We obtain the increments in LV pressure (Δp) from the monitored pressure data, during isovolumic contraction. By taking $K=\Delta p/\Delta V$, we compute the corresponding changes in LV volume ΔV.

2. Left ventricular deformation: For this change ΔV in the LV volume, by assuming the ratios of cylindrical-model length and radius strains $\Delta l/L$ and $\Delta r/R$ to be equal during isovolumic contraction, we obtain their expressions as:

$$\Delta l_j = \left(1 - \sqrt[3]{1 - \Delta p/K}\right)L, \quad \Delta r_{ij} = \left(1 - \sqrt[3]{1 - \Delta p/K}\right)R \tag{13}$$

From equation (13), the incremental quantities Δl_j and Δr_{ij} can be calculated, and hence:

$$l_j = L - \Delta l_j, \text{ and } r_{ij} = R - \Delta r_{ij} \tag{14}$$

where l_j and r_{ij} are the deformed model length and radius at time t (or j)
So the wall-thickness h can be obtained from:

$$h_j = \sqrt{\frac{V_M / l_j + \pi r_{ij}^2}{\pi}} - r_{ij} \tag{15}$$

Let $\Delta \phi$ denote the relative angle of twist measured at the apex, at each of the 3 stages of isovolumic contraction phase, obtained by magnetic resonance imaging (MRI).

3. Next we determine the stretches in the 3 directions (due to deformed dimensions l and r with respect to the undeformed dimensions L and R) as follows

$$\lambda_z(r) = \frac{1}{L}, \quad \lambda_r(r) = \frac{\partial r}{\partial R} = \frac{R}{r\lambda_z}, \quad \lambda_\theta(r) = \frac{r\partial\theta}{R\partial\Theta} = \frac{r}{R} \tag{16}$$

We define the twist stretch due to torsion, as

$$\gamma(r) = \frac{r\partial\theta}{\partial z} = \frac{r\phi}{l} \tag{17}$$

wherein ϕ is zero at the top surface of the LV held by the aorta

4. Next we express the components of the Lagrange Green's strain tensor in terms of the stretches and deformations obtained from equations (8-10), as:

$$E_{rr} = \frac{1}{2}\left(\lambda_r^2 - 1\right), \ E_{\theta\theta} = \frac{1}{2}\left(\lambda_\theta^2 - 1\right), \ E_{zz} = \frac{1}{2}\left(\lambda_z^2\left(1+\gamma^2\right) - 1\right), \ E_{\theta z} = \frac{\gamma\lambda_z\lambda_\theta}{2} \quad\quad (18)$$

5. Then, by using the strain energy function (eqs 5 and 6), we obtain the expressions of Cauchy stress tensor in terms of the parameters b_i:

$$\sigma_{\theta\theta} = \lambda_\theta^2\frac{\partial\Psi}{\partial E_{\theta\theta}} + 2\gamma\lambda_z\lambda_\theta\frac{\partial\Psi}{\partial E_{\theta z}} + \gamma^2\lambda_z^2\frac{\partial\Psi}{\partial E_{zz}} - \overline{p} \quad\quad \sigma_{rr} = \lambda_r^2\frac{\partial\Psi}{\partial E_{rr}} - \overline{p}$$

$$\sigma_{zz} = \lambda_z^2\frac{\partial\Psi}{\partial E_{zz}} - \overline{p} \quad\quad \sigma_{\theta z} = \lambda_z\lambda_\theta\frac{\partial\Psi}{\partial E_{\theta z}} + \gamma\lambda_z^2\frac{\partial\Psi}{\partial E_{zz}} \quad\quad (19)$$

wherein ψ is given by equations (5 & 6), and the to-be-determined unknown parameters are the hydrostatic pressure $\overline{p}$ and the constitutive parameters b_i (in equation 6).

6. We now employ the stress expressions into the boundary conditions (10 & 11), and determine the hydrostatic pressure $\overline{p}$ and the parameters b_i (i=1,2,…7) and, using a nonlinear least squares algorithm.

7. We next determine (i) the stretches from eqs (16 & 17), and (ii) therefrom, the strains $E_{i,j}$ from eq (18). Then by substituting the computed strains components $E_{i,j}$ and the strain energy density function ψ (eqs 5 & 6) into eq (19), we can determine the LV wall stress components for the LV cylindrical model.

8. From the stress components $\sigma_{\theta z}$, $\sigma_{\theta\theta}$, and σ_{zz}, we can computes the principal stresses σ_1, σ_2 the principal angle ϕ.

$$\sigma_{1,2} = \frac{\sigma_{zz} + \sigma_{\theta\theta}}{2} \pm \sqrt{\left(\frac{\sigma_{zz} - \sigma_{\theta\theta}}{2}\right)^2 + \sigma_{\theta z}^2}$$

$$(20)$$

$$\tan 2\phi = \frac{2\sigma_{\theta z}}{\sigma_{\theta\theta} - \sigma_{zz}} \quad\quad (21)$$

9. Then, we compute the equivalent active axial force ΔF and the torsional couple ΔT as follows:

$$\Delta F = 2\pi\int_{r_i}^{r_o}\sigma_{zz}r\,\mathrm{d}r, \quad M_T = 2\pi\int_{r_i}^{r_o}\sigma_{\theta z}r^2\,\mathrm{d}r, \quad\quad (22)$$

Results and comments:

1. The computational model results for a sample subject are provided in Tables 1 -5.
2. The variations of the equivalent active torque T and axial compressive force F during the isovolumic phase are calculated and shown in Fig. 12.
We hence demonstrate that the big increment of internal pressure in LV cavity is caused by the compression of the blood (due to its high bulk modulus) by the internally generated torque and axial force during the isovolumic phase, due to the contraction of the myocardial fibers.
3. The radial variations of the principal stress and principal angle are found to be almost uniform across the wall thickness [5]. The time variation of the principal stress and angle during isovolumic phase are shown in **Fig. 13**. At the end of the isovolumic phase, the magnitude of the tensile principal stress is around 1.75×10^5pa, which is in good agreement with the isometric tension value of 1.40×10^5pa achieved under maximal activation.
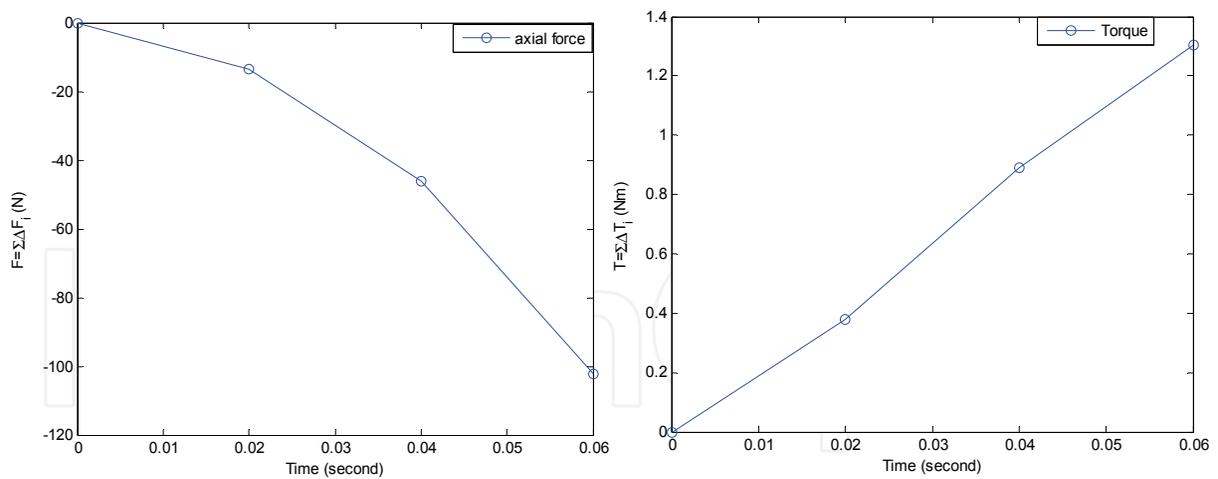
Fig. 12. Variations of axial force and torque as function of time during isovolumic phase [5].

The notable result from **Fig. 13** is that both the principle stresses and their orientation angle keep changing during the isovolumic phase. It is seen from Figure 13, that the myocardial fiber was oriented 38^0 at the start and became 33^0 at the end of the isovolumic phase, as the monitored internal pressure increased during isovolumic phase (due to active torsion and compression, corresponding to active contraction of the helically woven fibers from 38^0 to 33^0) from 24 to 44 to 62 mmHg during the isovolumic contraction phase. Observing the values of the principle stresses, it is seen that the LV is acted upon by internally generated (i) active torsion (T) causing its twisting, and (ii) compression (F) to cause compression of the blood and develop the LV pressure rise.
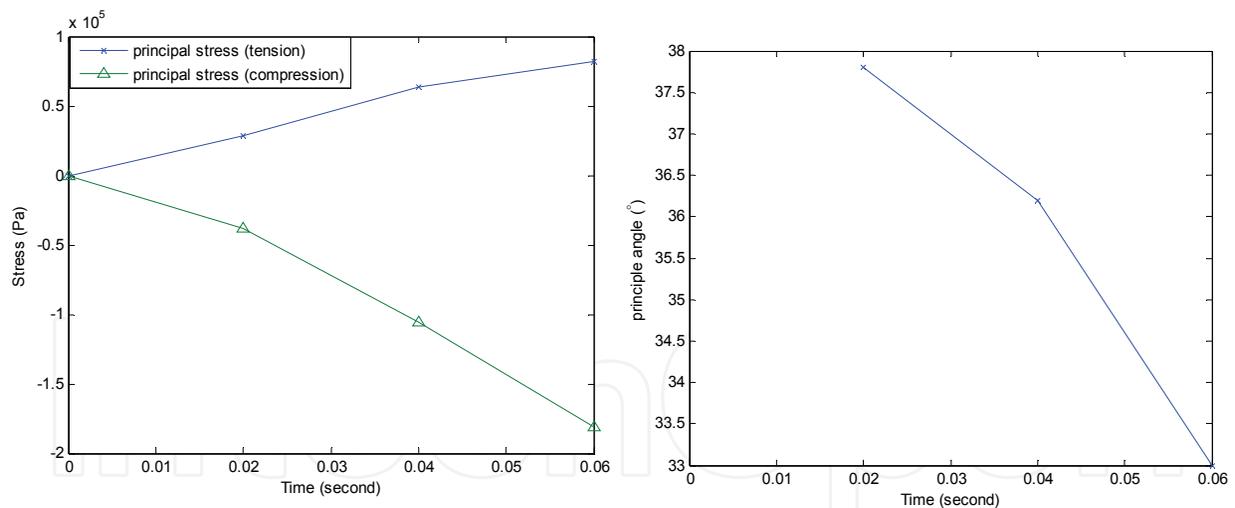
Fig. 13.Variation of principal stresses as functions of time, during isovolumic phase [5].

In conclusion: we have indirectly shown that the contraction of the myocardial fibers (i) develops active stresses in the LV wall (and corresponding principal stresses), and (ii) causes LV twist and shortening, resulting in the development of substantial pressure increase during isovolumic contraction.

The tensile principal stress corresponds to the active contractile stress generated in the myocardial fibers, while the angle of the tensile principal stress corresponds to the fiber helical angle, which is in agreement with the experiment data on the fiber angle.

The computational results are shown in Tables 1 to 5, for a sample subject.

Table 1. Pressure-volume and model parameters for a sample subject with V_M=185ml.

t (second)	P (mmHg)	ΔP (mmHg)	V (ml)	ΔV (ml)	r_{ij} (cm)	Δr_{ij} (cm)	l_j (cm)	Δl_j (cm)	
0	18		1.36700000E+02		2.03208400E+00 (=R_i)		1.053745000E+01 (=L)		1.085
0.02	43	25	1.36699773E+02	2.27263750E-04	2.032083992E+00	8.46701669E-09	1.053744996E+01	4.39060418E-08	1.085
0.04	63	45	1.36699591E+02	4.09074750E-04	2.032083985E+00	1.52406301E-08	1.053744992E+01	7.90308757E-08	1.085
0.06	81	63	1.36699427E+02	5.72704650E-04	2.032083979E+00	2.13368822E-08	1.053744989E+01	1.10643226E-07	1.085

parameter	b₁	b₂	b₃	b₄	b₅	b₆	b₇	b₈	b₉
value	5946.2278	15690.58158	422.514993	16157.10454	16360.53744	33299.28998	680.7385218	0	0

Table 2. The parameters of the strain energy function for the sample case shown in Table 1.

t	λ_z	λ_r	λ_θ	Υ
0				
0.02	0.9999999958	1.000000008E+00	9.99999996E-01	1.28626948E-01
0.04	0.9999999925	1.000000015E+00	9.99999993E-01	2.56482520E-01
0.06	0.9999999895	1.000000021E+00	9.99999990E-01	3.85688000E-01

Table 3. The stretches calculated from equations (16 & 17) for the sample case shown in Table 1.

t (second)	Endocardium---Epicardium									
	0	1.99E-02	1.02E-01	2.37E-01	4.08E-01	0.591715	0.762765	0.89833	0.98014	1
0.02	-24.0809	-23.4615	-17.2801	-12.9839	-8.73378	-4.9888	-2.11726	-0.41173	-0.2144	0
0.04	-44.2917	-43.1341	-31.6543	-23.7482	-15.9694	-9.13029	-3.88098	-0.75569	-0.3542	0
0.06	-6.21E+01	-6.05E+01	-5.43E+01	-4.48E+01	-3.39E+01	-2.31E+01	-1.34E+01	-5.75E+00	-1.13E+00	0

Table 4. Radial stresses distributions along LV wall from endocardium to epicardium.

t (second)	Results								
	Circumferential stress (Pa)	Radial stress (Pa)	Axial force (N)	Torque (Nm)	Axis stress (Pa)	Shear stress (Pa)	Principal stress-tension (Pa)	Principal stress-compression (Pa)	Principal direction (°)
0	0.00	0.00	0.00	0.00	0.00E+00	0.00E+00	0.00	0.00	
0.02	3358.33	-2844.53	-13.51	0.38	-1.35E+04	3.29E+04	28221.68	-38395.38	37.82
0.04	5318.61	-5956.38	-46.06	0.89	-4.70E+04	8.21E+04	63836.28	-105547.96	36.18
0.06	4481.83	-8530.94	-102.38	1.30	-1.04E+05	1.22E+05	81673.18	-180897.35	33.02

Table 5. Results for the sample subject at different instants

4. Clinical evaluation of Physiological systems in terms of Non-dimensional physiological Indices

Non-dimensional numbers (made up of several phenomenon related terms) are employed to characterise – disturbance phenomena. For example, in a cardiovascular fluid-flow regime, the Reynold's number

$$N_{re} = \rho V D / \mu \qquad (1)$$

(V : flow velocity, *D:* diameter, μ: fluid viscosity, ρ: fluid density)*

characterizes turbulent flow, which can occur in the ascending aorta when the aortic valve is stenotic (giving rise to murmurs) and accentuated in the case of anaemia (decreased blood viscosity).

Integration of a number of isolated but related events into one non-dimensional physiological index (NDPI) can help to characterise an abnormal state of a particular physiological system [1].

For utilization of an NDPI diagnostically, we evaluate it in a large patient population and develop its distribution into normal and dysfunctional ranges, as illustrated in figure 14. Then, upon evaluation of the NDPI of a particular subject, we can see if that value falls in the normal or dysfunctional range, and accordingly make the medical diagnosis.
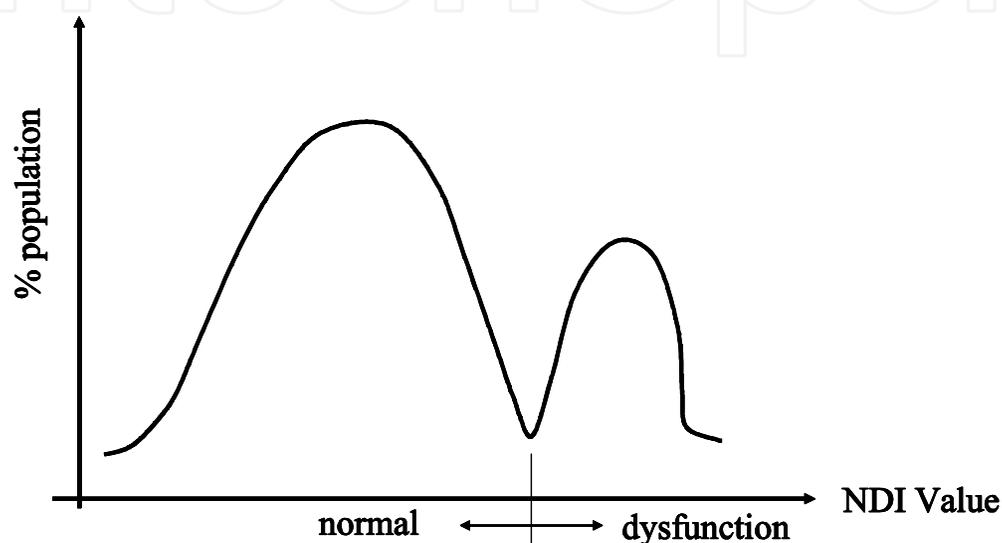
Fig. 14. Illustration of the Distribution of an NDI, showing its normal and dysfunctional ranges which can be employed for diagnostic purpose.

5. Medical test: Cardiac fitness index based on treadmill HR variation

In this procedure, the cardiac fitness model consists of a first-order differential-equation system model, describing the heart rate (HR) response (y) to exertion (exercise, jogging etc) monitored in terms of the work-load, where y is defined as follows:

$$y = \frac{HR(t) - HR(rest)}{HR(rest)} \tag{1}$$

The subject is exercised on the treadmill for a period of time *te* (minutes) at a constant work load (W), while the HR(t) (and hence y) is monitored, as displayed in fig 15. Now we develop a model to simulate (i) the y(t) response during exercise, i.e. during $t \leq te$, and (ii) thereafter for y(t) decay, after the termination of exercise. In a way, *te* represents the exercise endurance of the subject [6].

For a person, the model equation for HR response is represented by:

$$\frac{dy}{dt} + k_1 y = C_0 W \tag{2}$$

For $t \leq t_e$, the solution is given by:

$$y = \frac{y_e(1 - e^{-k_1 t})}{(1 - e^{-k_1 t_e})} \tag{3}$$

For the recovery period $(t \geq te)$, the solution of eqn. (2) is :

$$y = y_e e^{-k_2(t - t_e)} \tag{4}$$

where k_1 and k_2, are the model parameters, which can serve as cardiac-fitness parameters (in min^{-1}).

Non-dimensional Cardiac Fitness Index:
A typical y(t) response is illustrated in Fig 15.
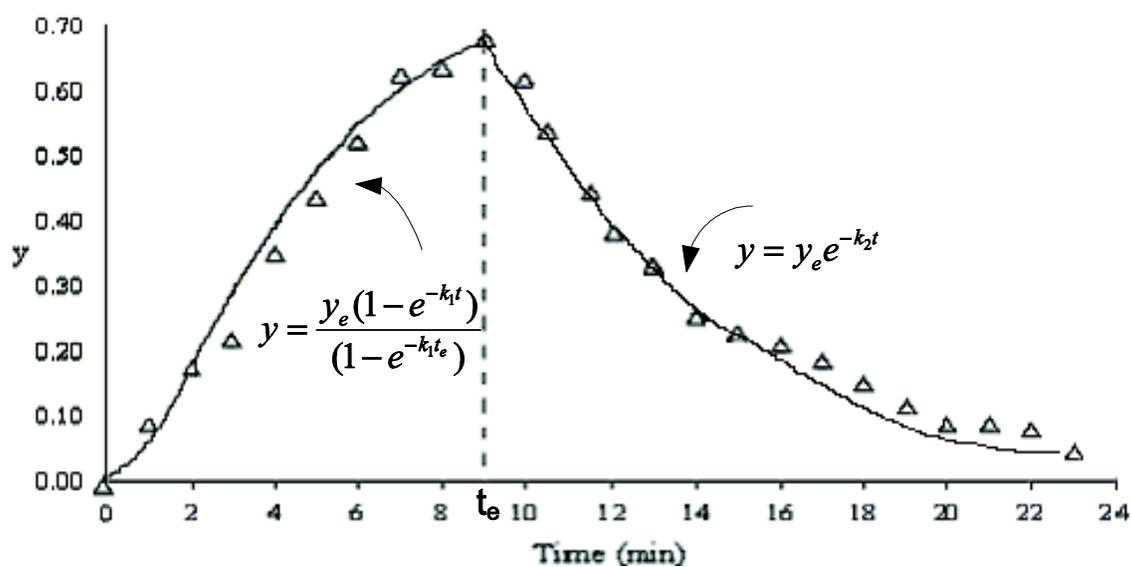
Fig. 15. Graph of y (the computed HR response) vs. t during treadmill exercise $t=te$ and during the recover of period $t=te$.

The parameters k_1 and k_2 can be continued into a single nondimensional cardiac-fitness index (CFI):

$$CFI = k_1 k_2 t_e^2 \tag{5}$$

According to this formulation of CFI, a healthier subject has (i) greater k_1 (i.e., slower rate-of-increase of HR during exercise (ii) greater k_2 (i.e., faster rate-of-decrease of HR after exercise) (iii) greater t_e (i.e., exercise endurance), and hence (iv) higher value of CFI.

Subject	Classification	CFI (relative values)
1	Athletic	271
2	Occasionally runs	90
3	Rarely exercise	65
4	Sedentary	19
5	Exercises regularly	155

Table 1. CFI values for athletic, fit and unfit subjects.

Now, we need to evaluate CFI for a big spectrum of patients, and then compute its distribution curve, to determine the efficiency of this index, in order to yield distinct separation of CFI ranges for healthy subjects and unfit patients. This CFI can also be employed to assess improvement in cardiac fitness following cardiac rehabilitation regime. This CFI is non-dimensional, and it can be useful to clinicians as they are able to predict the heart condition or fitness performance of a person by referring to the value of a single index value.

6. Medical physiology: A non-dimensional diabetes index with respect to Oral-Glucose-Tolerance testing

$y(t) = \dfrac{G}{\omega} e^{-At} \sinh \omega t$

$(AT_d = 4.9)$

$\lambda = 0.27 hr^2$

$T_d = 6.08 hr$

$G = 2.84 gmlit^{-1} hr^{-1}$

$A = 0.808 hr^{-1}$

$y(t) = \dfrac{G}{\omega} e^{-At} \sin \omega t$

$(AT_d = 1.4)$

$\lambda = 2.6 hr^2$

$T_d = 1.08 hr$

$G = 1.04 gmlit^{-1} hr^{-1}$
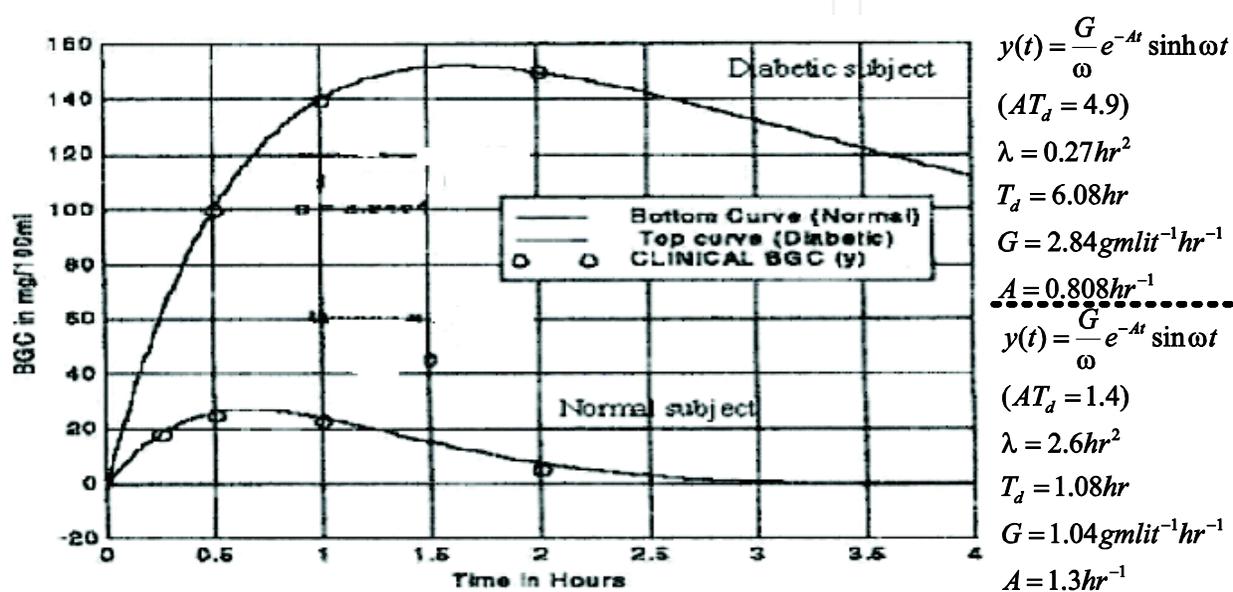
$A = 1.3 hr^{-1}$

Fig. 16. OGTT response-Curve: A=1.3hr-1 (i.e., higher damping.coefficient value) for the normal subject for the diabetic patient A=0.808 hr-1, i.e., the damping coefficient is smaller [7, 8].

Oral Glucose Tolerance Test (OGTT) is a standard procedure for diagnosing diabetes and risk of becoming diabetic. However, the test data is assessed empirically. So, in order to make this procedure more reliable, we have carried out a biomedical engineering analysis of the OGTT data, to show how to distinguish diabetes subjects and those at risk of becoming diabetic.
For Oral-glucose Tolerance Test simulation (entailing digestive & blood-pool chambers), the differential equation is as follows [7,8]:

$$y'' + 2Ay' + \omega_n^2 y = G\delta(t); \quad \text{y in gms/liter, G in gm/liter/hr}$$
$$or,$$
$$y'' + \lambda T_d y' + \lambda y = G\delta(t)$$

(1)

wherein $\left(\omega_n = \lambda^{1/2}\right)$ is the natural oscillation-frequency of the system, A is the attenuation or damping constant of the system, $\omega = (\omega_n^2 - A^2)^{1/2}$ is the (angular) frequency of damped oscillation of the system, $\lambda = 2A/T_d =, \vee \omega_n^2$ with (λy) representing the proportional-control term of blood-glucose concentration (y).

($\lambda T_d y'$)is the derivative feedback control term with derivative-time of T_d $G\delta(t)$ represents the injected glucose bolus.

The input to this system is taken to be the impulse function due to the orally ingested glucose bolus [G], while the output of the model is the blood-glucose concentration response y(t). For an impulse glucose-input, a normal patient's blood-glucose concentration data is depicted in **Figure 16** by open circles. Based on the nature of this data, we can simulate it by means of the solution of the Oral-glucose regulatory (second-order system) model, as an under-damped glucose-concentration response curve, given by:

$$y(t) = (G / \omega)e^{-At}\sin\omega t, \tag{2}$$

$$\omega = \left(\omega_n^2 - A^2\right)^{1/2}$$

wherein A is the attenuation constant, is the damped frequency of the system, thenatural frequency of the system = ω_n, and $\lambda = 2A/T_d$.

The model parameters λ and T_d are obtained by matching eqn.(1) to the monitored glucose concentration y(t) data (represented by the open circles). The computed values of parameters are: λ = 2.6 hr^{-2}, T_d = 1.08 hr. This computed response is represented in Figure 1 by the bottom curve, fitting the open-circles clinical data.

ParametricIdentification (sample calculation for Normal Test Subject No.5)

$$y(1/2) = (G / \omega)e^{-A/2}\sin\omega / 2 = 0.34 \text{ g} / \text{L}$$

$$y(1) = (G / \omega)e^{-A}\sin\omega = 0.24 \text{ g} / \text{L}$$

$$y(2) = (G / \omega)e^{-2A}\sin 2\omega = -0.09 \text{ g} / \text{L}$$

Using trignometry relations, we get

$$A = 0.8287 \text{ hr}^{-1}$$

$$\lambda = \omega_n^2 = A^2 + \omega^2 = (0.82875)^2 + (2.0146)^2 = 4.7455 \text{ hr}^{-2},$$

$$T_d = 2A / \lambda = 0.3492 \text{ hr}$$

Upon substituting the above values of λ and Td, the value of the third parameter,

$$G = 1.2262 \text{ g} (1)^{-1} \text{hr}^{-1}$$

For a diabetic subject, the blood-glucose concentration data is depicted by closed circles in Fig 16. For the model to simulate this data, we adopt the solution of model eqn(17), as an over-damped response function:

$$y(t) = (G / \omega) e^{-At}\sinh\omega t \tag{3}$$

The solution ($y = (G/ \omega) e^{-At}\sinh\omega t$) is made to match the clinical data depicted by closed circles, and the values of λ and T_d are computed to be 0.27 hr^{-2} & 6.08 hr, respectively. The

top curve in **Figure 16** represents the blood-glucose response curve for this potentially diabetic subject. The values of T_d, λ and A for both normal and diabetic patients are indicated in the figure, to provide a measure of difference in the parameter values.

It was found from these calculations that not all of the normal test subjects' clinical data could be simulated as under-damped response. Similarly, not all the diabetic test subjects' clinical data corresponded to over-damped response.

However it was found that the clinical data of these test subjects (both normal and diabetic) could indeed be fitted by means of a critically-damped glucose-response solution of the governing equation.

$$y(t) = G\, t\, e^{-At} \tag{4}$$

for which, $\omega = 0$, $\omega_n^2 = A^2 = \lambda$, and $T_d = 2A/\lambda = 2$

Clinically-based Diagnosis:

The blood glucose 'normal' values, used for the clinical studies, were: Fasting: 70 to 115 mg/dl, At 30th min.: less than 200 mg/dl,

At 1st hour: less than 200 mg/dl, At 2nd hour: less than 140 mg/dl,

Modeling-based Diagnosis:

The test subjects have been classified into four categories:

Normal-test subjects based on under-damped model-response;

Normal test-subjects based on critically-damped model-response, at risk of becoming diabetic;

Diabetic test-subjects based on critically-damped model-response, being border-line diabetic;

Diabetic test-subjects based on over-damped model response;

Non-Dimensional Number for Diagnosis of diabetes:

We decided to develop a unique diabetes index number (DIN) to facilitate differential diagnosis of normal and diabetic states as well as diagnose supposedly normal but high (diabetic) risk patients and diabetic patients in early stages of the disorder [8].

$$\text{DIN} = \frac{y(\max)}{G} \times A \times \frac{T_d}{T(\max)} \tag{5}$$

wherein,

y(max) = maximum blood glucose value in gram/liter

G = glucose dose administered to the system in gram/liter hour

A = attenuation constant in 1/hour

T_d = derivative-time ($\alpha + \delta$) in hours

T(max) = the time at which y(max) is attained in hour

This non-dimensional number DIN consists of the model parameters (A & T_d) or (A & ω_n) or (λ & T_d). The DIN values for all four categories were computed from equation (5). A distribution plot of the DIN is plotted in fig 17, wherein the DIN is classified into sections with 0.2 increments (for all the four categories of subjects) and the number of subjects which fall into these sections (frequency) is determined.

In the distribution plot (shown in Fig 17), the DIN values 0-0.2 is designated as range 1, the DIN 0.2-0.4 is range 2, 0.4-0.6 is range 3, and so on up to DIN 2.2-2.4, which is range 12.

As can be seen from figure 17, normal (i.e., non-diabetic) subjects with no risk of becoming diabetic, will have DIN value less than 0.4, or be in the 1 – 2 range. Distinctly diabetic subjects will have DIN value greater than 1.2, or be in the 7 – 12 range categories.

Supposedly, clinically-identified normal subjects who have DIN values between 0.4 and 1.0, or are in the 3 – 5 range, are at risk of becoming diabetic.

On the other hand, clinically-identified diabetic subjects with DIN value between 0.4 – 1.2, or in the 3 – 6 range category are border-line diabetics, who can become normal (with diet control and treatment).
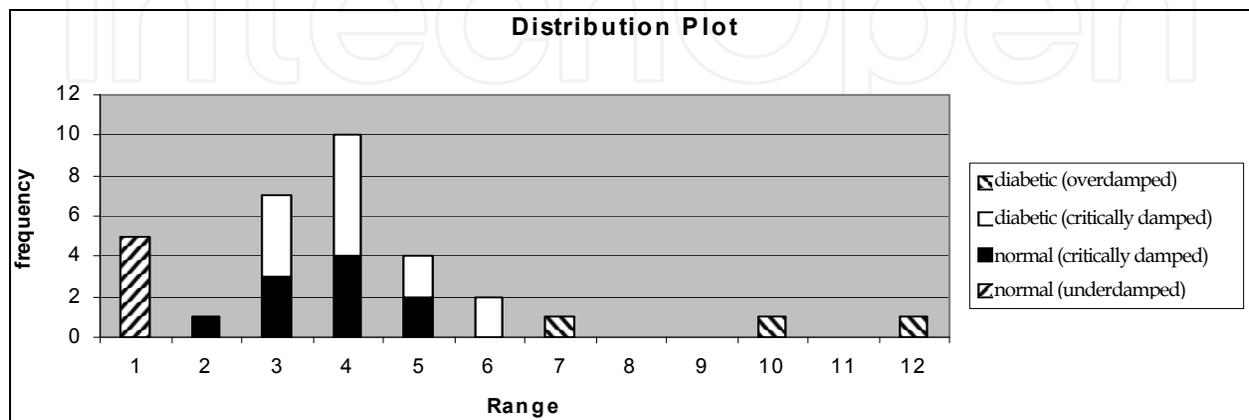
Fig. 17. DIN distribution plot of all the four categories subjects [8]. In the figure, diabetic (critically damped) category of subjects are designated as border-line diabetic; normal (critically damped) category of subjects are designated as normal subjects at risk of becoming diabetic.

7. Cardiology: LV contractility index based on normalized wall-stress

The traditional cardiac contractility index $(dP/dt)_{max}$ requires cardiac catheterization.
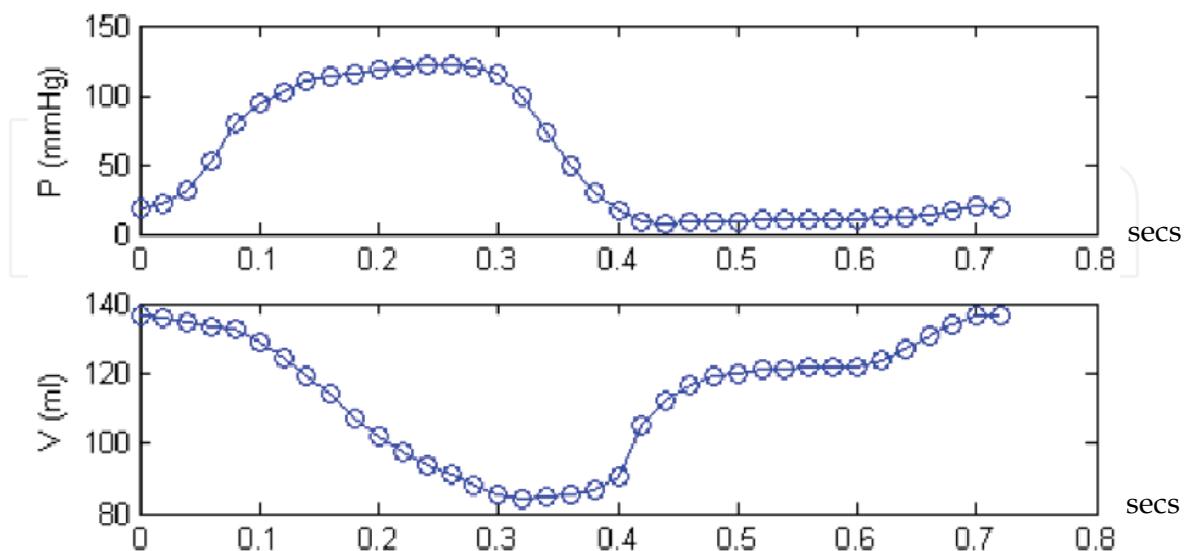
Fig. 18. Sample cyclic variation of LV pressure and volume.

Since LV Pressure is developed by LV wall stress σ_θ(based on sarcomere contraction), we have developed a contractility index based on σ_θ (normalized with respect to LV pressure) [9].

For a thick walled spherical model of LV, the circumferential wall stress:

$$\sigma_\theta(r_i) = P\frac{(r_i^3 / r_e^3 + 0.5)}{(1 - r_i^3 / r_e^3)} \tag{1}$$
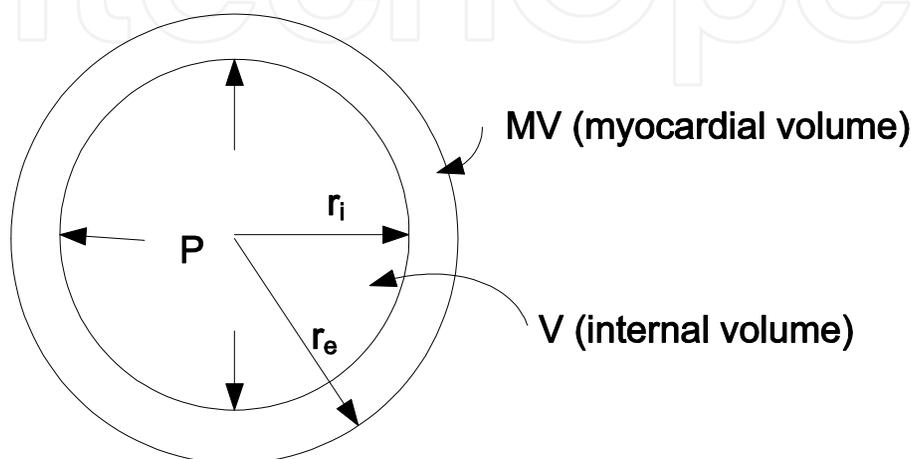
Fig. 19. Thick walled Spherical Model of the LV.

$$\text{The normalised Stress} = \frac{\sigma_\theta(r_i)}{P} = \sigma^* = \frac{3V}{2MV} + \frac{1}{2} \tag{2}$$

We define the contractility index as:

$$\text{Contractility Index (CONT1)} = \left|\frac{d\sigma^*}{dt}\right|_{max} = \frac{3}{2MV}\left(\frac{dV}{dt}\right)_{max} \tag{3}$$

For the data shown in the figure 18, we have:

$$CONT1 = \frac{3}{200cc}(224cc \cdot s^{-1}) = 3.3s^{-1}$$

Now we formulate a non-dimensional cardiac contractility index,

$$CONT2 = \left|\frac{d\sigma^*}{dt}\right|_{max} \times ejection\ period(= 0.3second) \times 100$$

$$\approx 100$$

Our new contractility indices do not require measurement of LV pressure, and can hence be evaluated noninvasively. In fig 20, we can see how well our contractility index $CONT1$ $(d\sigma^*/dt)_{max}$ correlates with the traditional contractility index $(dP/dt)_{max}$. This provides a measure of confidence for clinical usage of this index.
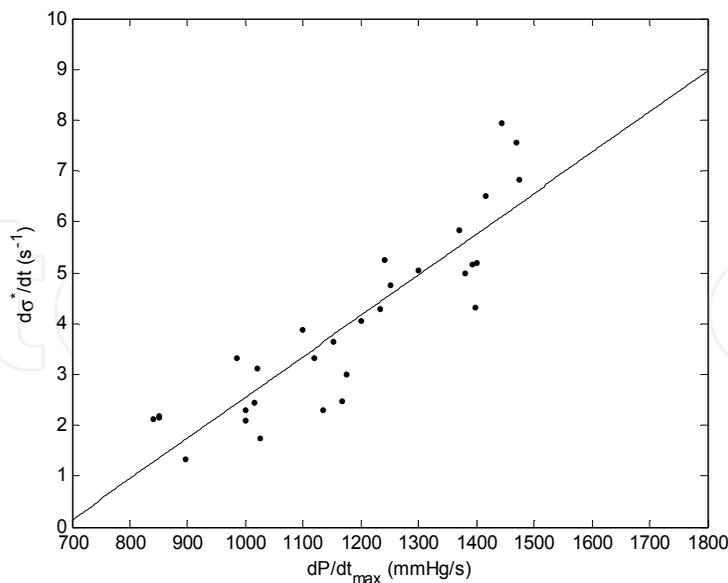
Fig. 20. Correlation of our new contractility index $(d\sigma^*/dt)_{max}$ with the traditional contractility index $(dP/dt)_{max}$

8. Diagnostics: LV contractility index based on LV shape-factor

Cardiologists have observed shape changes taking place in an impaired LV. We have investigated the effect of ventricular shape on contractility and ejection function. In this study, a new LV contractility index is developed in terms of the wall-stress (σ^*, normalized with respect to LV pressure) of a LV ellipsoidal model (Fig. 21) [10, 11].

Using cine-ventriculography data of LV volume (V) and myocardial volume MV, the LV ellipsoidal model (LVEM) major (B) and minor axes (A) are derived for the entire cardiac cycle. Thereafter, our new contractility index $(d\sigma^*/dt)_{max}$ is derived in terms of the LV ellipsoidal shape factor $(s=B/A)$.

For the LV model (Fig 21) of a prolate spheroid truncated 50% of the distance from the equator to the base, we first put down the for σ^* ($= \sigma_\theta /P$), and then determine $d\sigma^*/dt$ [2.10]. Thereby, we obtain the following expression for the contractility index:

$$Contractility\ index - 1\ (CONT1) = \left| (d\sigma^* / dt) \right|_{max}$$

$$= \left| \frac{\dot{V}(2+s) + V\dot{s}}{MV} - \frac{V^2 s}{MV(4V+2Vs+MV)^2} \left(\begin{array}{c} s\dot{V}(8+4MV/V+(8+2MV/V)s+2s^2) \\ +V\dot{s}(16+4MV/V+(16+3MV/V)s+4s^2) \end{array} \right) \right|_{max} = F(s,\dot{s},V,\dot{V},MV)$$

where s is B/A, ś is first-time derivative of s; V and MV are LV volume and myocardial wall volume, $\tilde{V}$ is the first-time derivative of V.

This index is analogous to the traditional employed index $(dP/dt)_{max}$, but does not involve determination of the intra-LV pressure by catheterization. For patient A (with myocardial infarct and double vessel disease) and B (with double vessel disease and hypertension), the values of CONT1 are obtained to be 3.84 and 6.90 s^{-1}, whereas the corresponding values of $(dP/dt)_{max}$ are obtained to be 985 and 1475 mmHg/s.

a   b

Comparison of the
constructed LV
ellipsoidal model
geometry with the
cineangiography
derived geometries:

(a) at an instant
during the diastolic
filling phase,

(b) at an instant
during the systolic
ejection phase,

(c) cineangiography
measured LV
dimensions,

(d) LV ellipsoidal
model geometry,
showing the model
geometrical
dimensions.

c   d
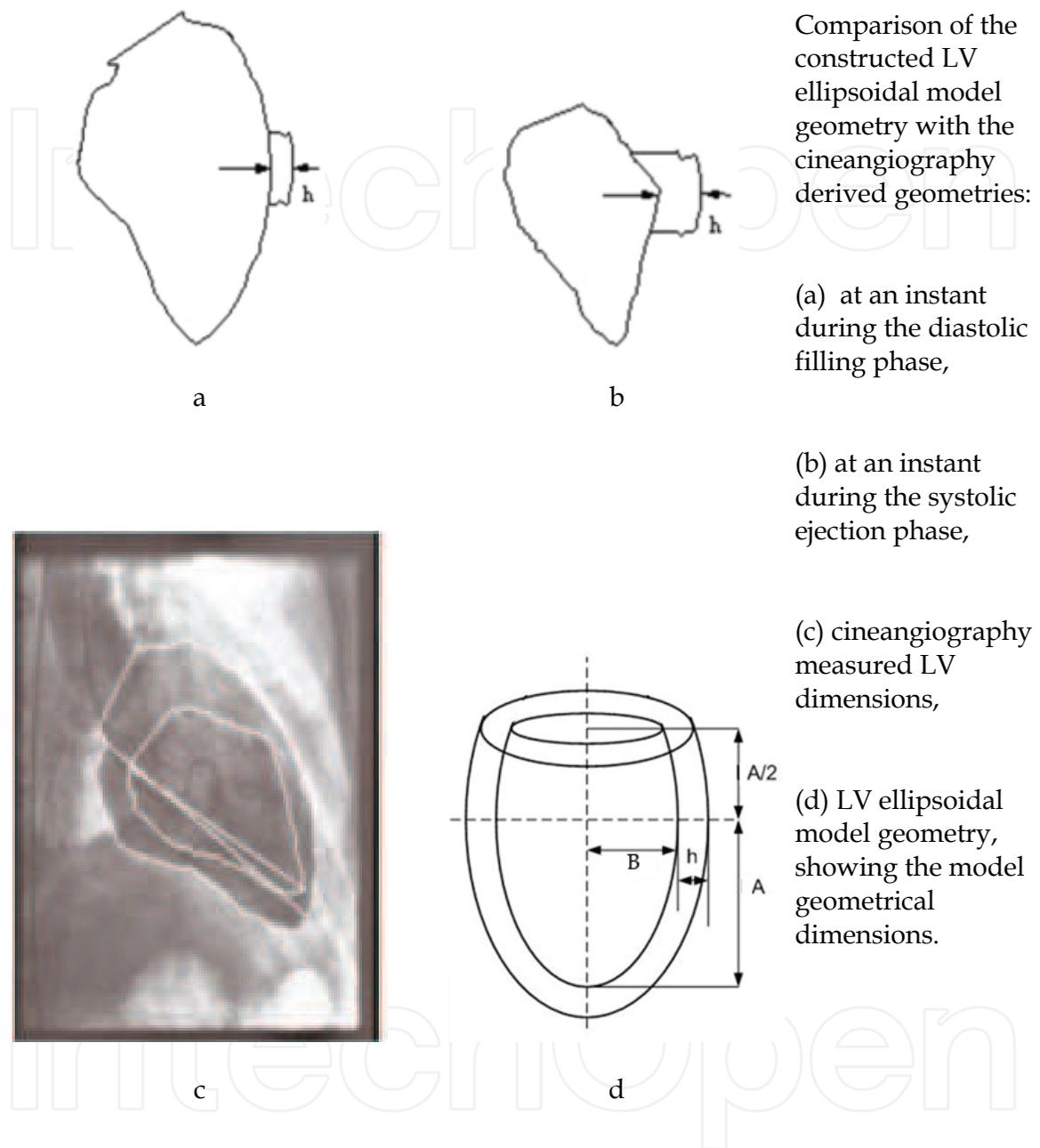
Fig. 21. Cineangiography imaged LV geometry and the corresponding constructed LV
ellipsoidal model: (a) at an instant during the diastolic filling stage, (b) at an instant during
the systolic ejection stage, (c) measured LV dimensions, (d) LV ellipsoidal model, depicting
its geometrical parameters.
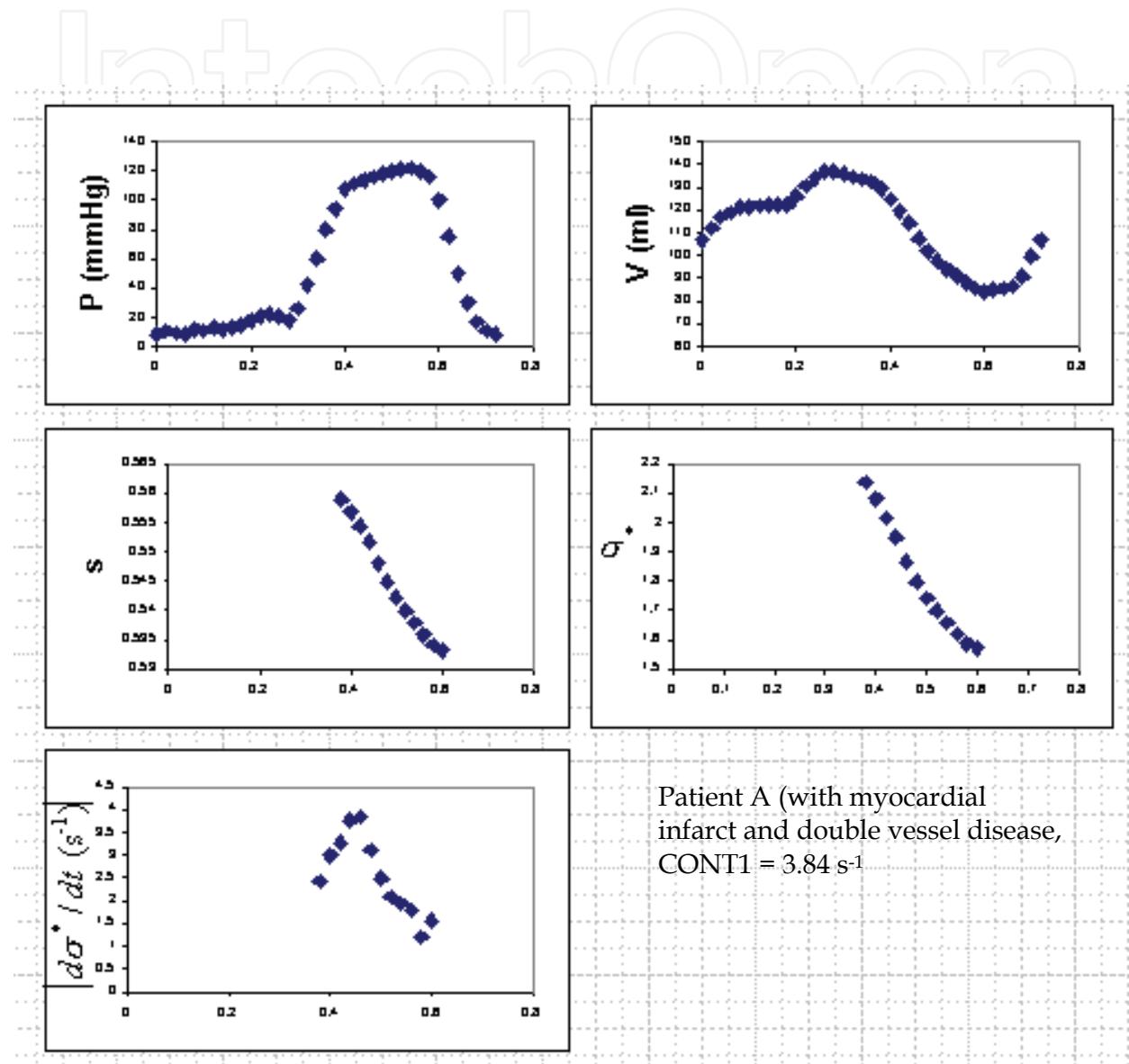
Fig. 22. Patient A: Cyclic variation of LV pressure-volume data, LV model shape factor s, computed σ*, computed index *(dσ*/dt)_{max}*.

Patient B (with double vessel disease and hypertension), CONT1 = 6.90 s^{-1}
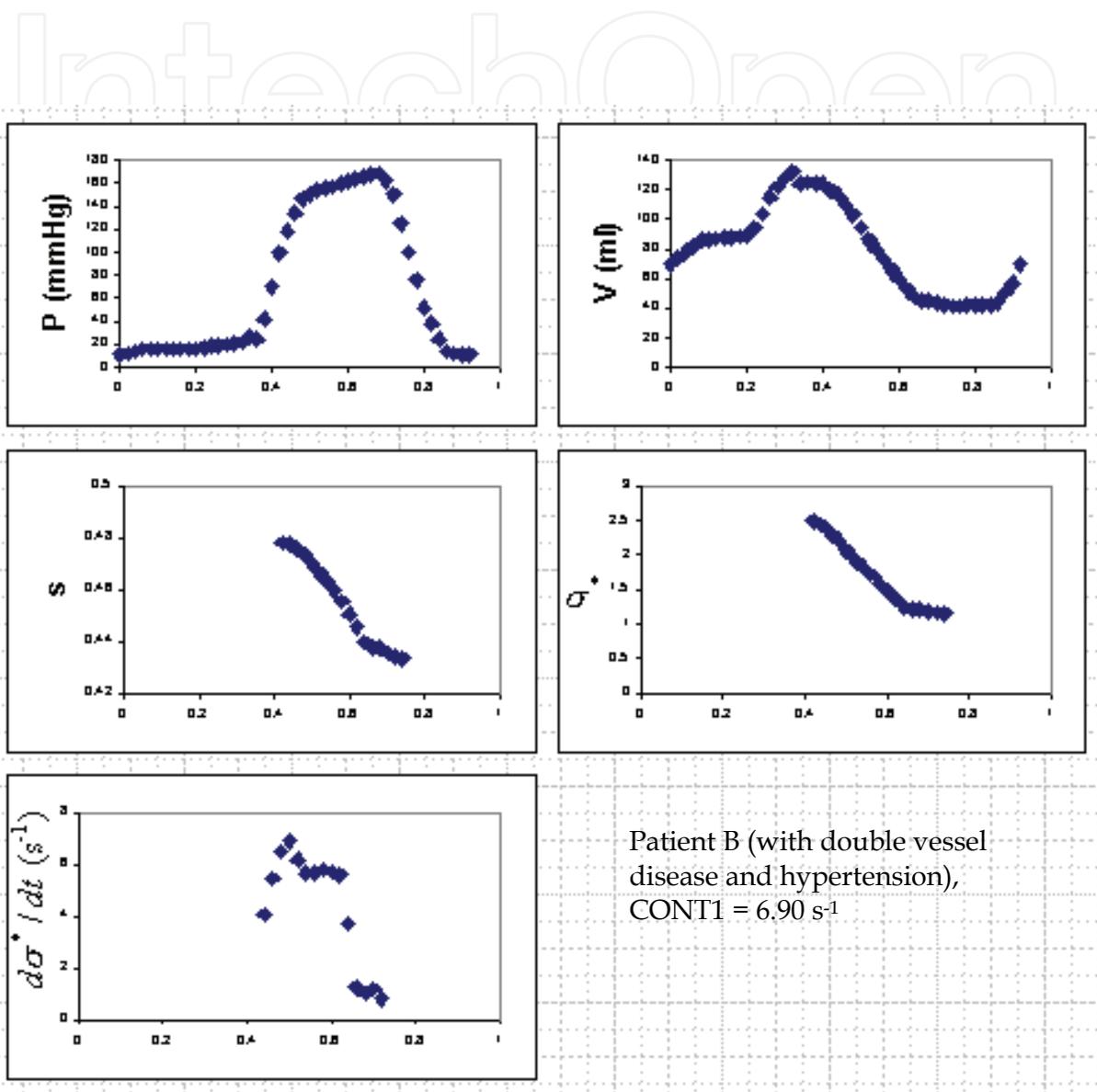
Fig. 23. Patient B: Cyclic variation of LV pressure-volume data, LV model shape factor s, computed σ*, computed index $(d\sigma^*/dt)_{max}$.
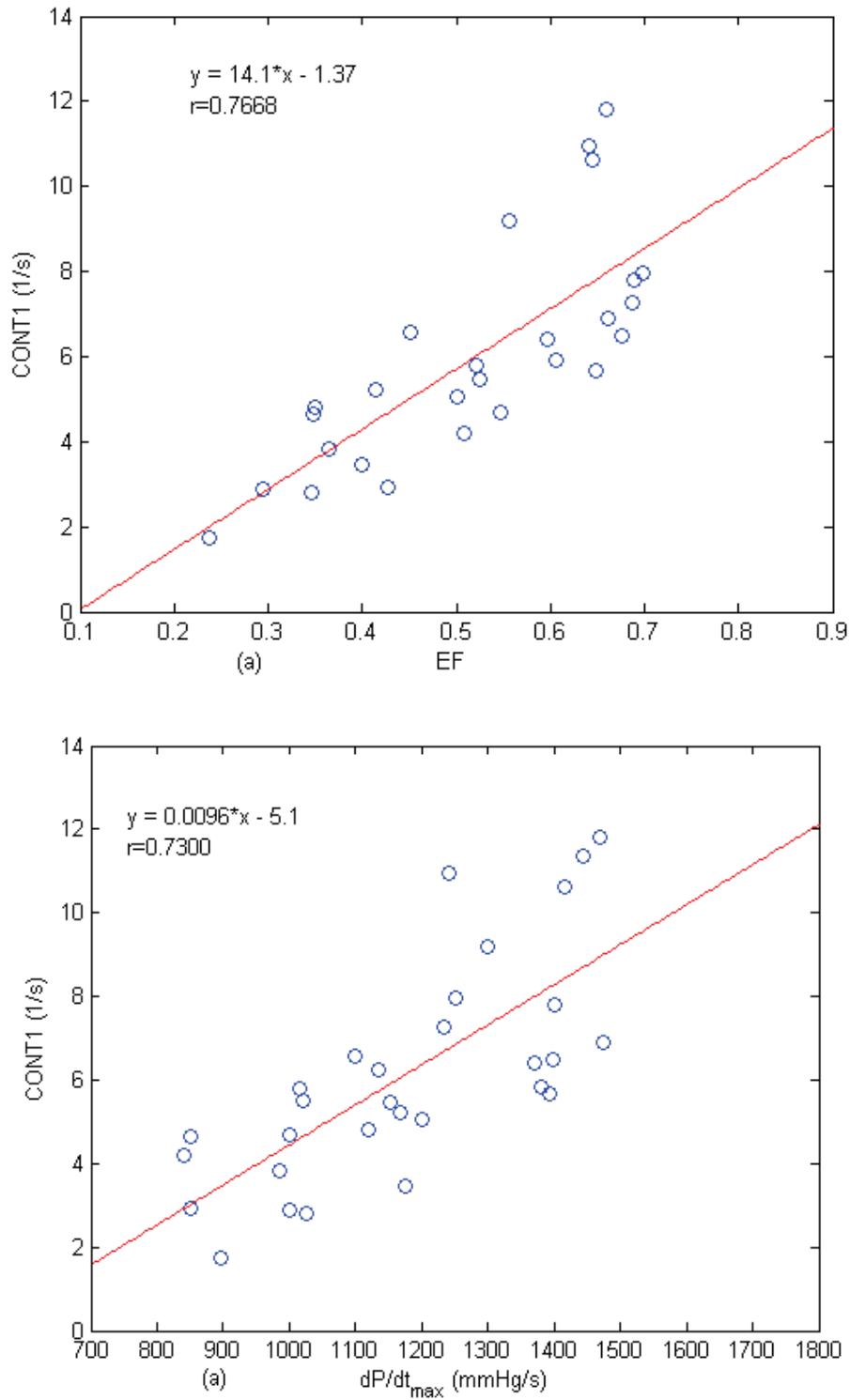
Fig. 24. Correlationships between (i) CONT1 and EF, and (ii) CONT1 and *(dP/dt)max*.

For our patient group, we have computed and plotted CONT1 vs EF and $(dP/dt)_{max}$ in Fig. 24. We can note the good level of correlation with the traditional contractility index of $(dP/dt)_{max}$. Additionally, our new index can be determined noninvasively, and hence be more conducive for clinical use.

From these results, we can also infer that a non-optimal less-ellipsoidal shape (or a more spherical shape, having a greater value of $S = B/A$) is associated with decreased contractility (and poor systolic function) of the LV, associated with a failing heart. This has an important bearing on a quick assessment of a failing heart based on the values of S and $(d\sigma^*/dt)_{max}$

9. ICU Evalution: Indicator for lung-status in mechanically ventilated copd patients (using lung ventilation modelling and assessment)

In chronic-obstructive-pulmonary-disease (COPD), elevated airway resistance and decreased lung compliance (i.e. stiffer lung) make breathing difficult. After these patients are mechanically ventilated, there is a need for accurate predictive indicators of lung-status improvement, for ventilator discontinuation through stepwise reduction in mechanical support, as and when patients are increasingly able to support their own breathing, followed by trials of unassisted breathing preceding extubation, and ending with extubation.

So, in this section, we have provided a biomedical engineering analysis of the lung ventilator volume response to mechanical ventilation of COPD patients, and developed an index to assess the lung status as well as the basis of weaning the patient from ventilator support.

Figure 25 depicts the model for the lung volume (V) response to the net driving pressure $P_N = P_L - P_e$ (end-expiratory pressure), in which (i) the driving pressure $P_L = P_m$ (pressure at the mouth) minus P_p (the pleural pressure), and (ii) P_p is determined by intubating the patient, and assuming that the pressure in the relaxed esophageal tube equals the pressure in the pleural space surrounding it.
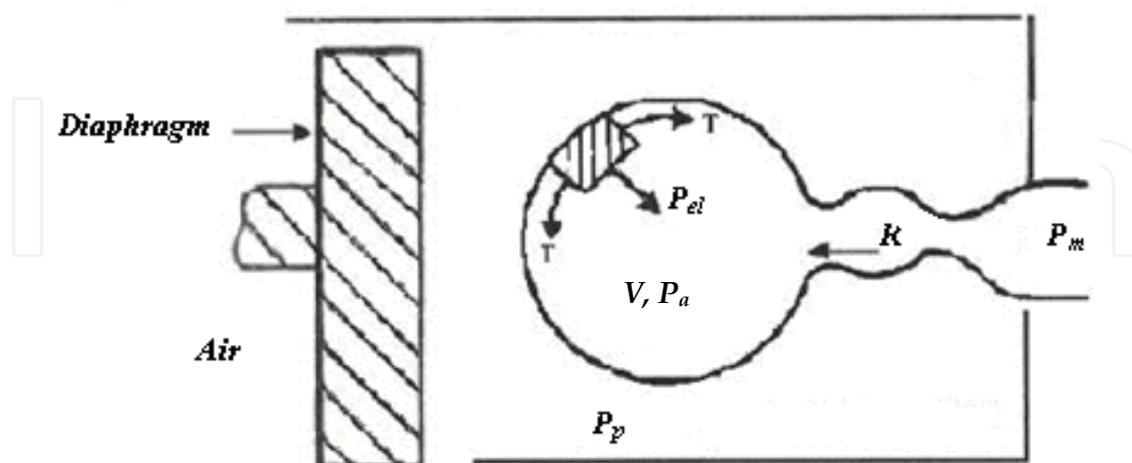

Fig. 25. Model of the Lung, depicting P_m, P_p, P_{el} (lung elastic pressure recoil) = P_a (alveolar pressure) – P_p (pleural pressure) = 2T/(radius of alveolar chamber), and
R (resistance to airflow rate) = $(P_m - P_a)$ / (dV/dt).

The equation representing the lung model response to the net driving pressure in terms of the model parameters lung compliance *(C)* and airflow-resistance *(R)*, is given by:

$$R\overset{o}{V} + \frac{V}{C} = P_L(t) - P_e = P_N(t) \tag{1}$$

wherein:

1. the driving pressure = P_L ; Pe = the end-expiratory pressure; net pressure $P_N = P_L - Pe$
2. the parameters of the governing equation (1) are lung compliance (C) and airflow-
3. resistance(R), with both R & C being instantaneous values
4. V= V(t) – Ve (wherein Ve is the end expiratory lung volume)
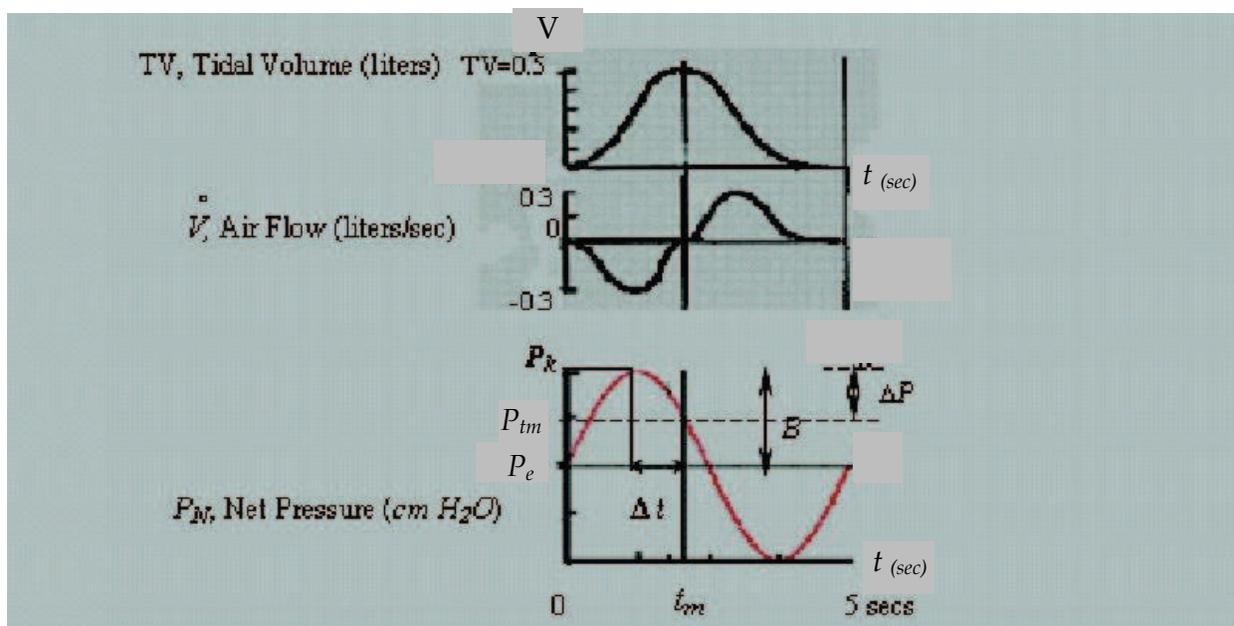
Fig. 26. Lung ventilatory model data shows air-flow ($\overset{o}{V}$) and volume (*V*) and net pressure (P_N). Pause pressure (P_{tm}) occurs at t_m, at which the volume is maximum (TV = tidal volume). Δt is the phase difference between the time of maximum volume and peak pressure (P_k). It also the time lag between the peak and pause pressures. *B* is the amplitude of the net pressure waveform P_N applied by the ventilator. This P_N oscillates about P_e with amplitude of *B*. The difference between peak pressure P_k and pause pressure P_{tm} is Δp [12].

We measure Peak pressure (P_k), Pause pressure (P_{tm}), t_m & ω (or $t_m \omega$).
Then,

$$P_k = P_L(t = \pi / 2\omega) = P_e + B$$
$$P_{tm} = P_L[t = t_m = (\pi - \theta) / \omega] = P_e + B\sin \omega t_m = P_e + B\sin[\omega(\pi-\theta)/\omega]$$
$$= P_e + B\sin(\pi - \theta) = P_e + B\sin\theta$$
$$\therefore B = (P_k - P_{tm})/(1 - \sin\theta) = \Delta P/(1-\sin\theta)$$

B is the amplitude of the net pressure wave form applied by the ventilator. Let C_a be the average dynamic lung compliance, R_a the average dynamic resistance to airflow, the driving pressure $P_L = P_e + B \sin(\omega t)$, and the net pressure $P_N = B \sin(\omega t)$. The governing equation (1) then becomes [12]:

$$R_a \overset{o}{V} + \frac{V}{C_a} = P_N = B\sin(\omega t) \tag{2}$$

The volume response to P_N, the solution to eqn (2), is given by:

$$V(t) = \frac{BC_a\{\sin(\omega t) - \omega k_a \cos(\omega t)\}}{1 + \omega^2 k_a^2} + He^{-t/k_a} \tag{3}$$

wherein:
    i.   ka (=RaCa)is the average time constant,
    ii.   the integration constant H is determined from the initial conditions,
    iii. the model parameters are Ca and ka(i.e. Ca and Ra), and
    iv. ω is the frequency of the oscillating pressure profile applied by the ventilator

An essential condition is that the flow-rate is zero at the beginning of inspiration and end of expiration. Hence, applying this initial condition of *dV/dt* =0 at t=0 to our differential eqn (3), the constant *H* is obtained as:

$$H = \frac{BC_a \omega k_a}{1 + \omega^2 k_a^2} \tag{4}$$

Then from eqn (3) & (4), we obtain:

$$V(t) = \frac{BC_a\{\sin(\omega t) - \omega k_a \cos(\omega t)\}}{1 + \omega^2 k_a^2} + \frac{BC_a \omega k_a}{1 + \omega^2 k_a^2} e^{-t/k_a} \tag{5}$$

Evaluating parameters R_a & C_a [12,2]:

For evaluating the parameter $k_a(R_aC_a)$, we will determine the time at which *V (t)* is maximum and equal to the tidal volume (TV), Hence putting *dV/dt* =0 in eqn (5), we obtain:
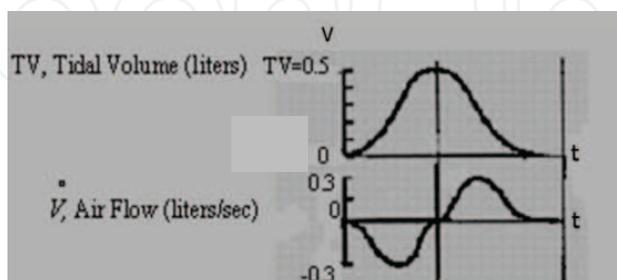
$$\cos(\omega t) + \omega k_a \sin(\omega t) = e^{\left(\frac{-t}{k_a}\right)}, \text{ at t = tm} \tag{6}$$

From equation (6), we obtain (by neglecting e^{-t/k_a}), the following expression for k_a:

PN, Net Pressure (cm H_2O)
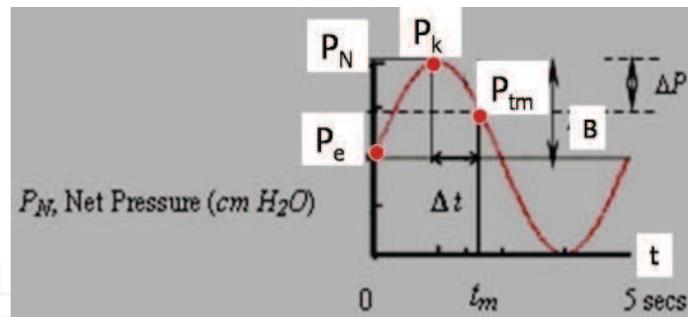
$$k_a = -1/\omega \tan(\omega t_m) \tag{7a}$$

$$or, \quad \tan^{-1}(1/\omega k_a) = \pi - (\omega t_m) = \theta \tag{7b}$$

From eqn (5 & 6):

$$V(t = t_m) = TV = \frac{BC_a\{\sin(\omega t_m) - \omega k_a \cos(\omega t_m)\}}{1 + \omega^2 k_a^2} + \frac{BC_a \omega k_a}{1 + \omega^2 k_a^2} e^{-t_m/k_a} \tag{8}$$

At $t = t_m$, the second term,

$$H = \frac{BC_a \omega k_a}{1 + \omega^2 k_a^2} e^{-t_m/k_a} \approx 0 \tag{9}$$

Hence, eqn (8) becomes:

$$V(t = t_m) = TV = \frac{BC_a\{\sin(\omega t_m) - \omega k_a \cos(\omega t_m)\}}{1 + \omega^2 k_a^2} \tag{10}$$

TV, Tidal Volume (liters)   TV=0.5

$\dot{V}$, Air Flow (liters/sec)
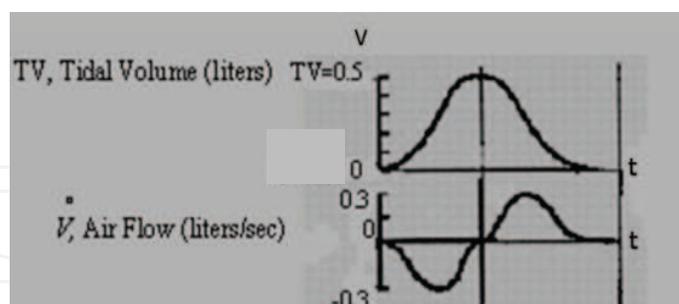
In eqn (10), if we put:

$$N = \sin(\omega t_m) - \omega k_a \cos(\omega t_m) \tag{11}$$

Then, based on equations (6 and 7), we get:

$$N = \frac{1}{\sqrt{1 + \omega^2 k_a^2}} + \frac{\omega^2 k_a^2}{\sqrt{1 + \omega^2 k_a^2}} = \sqrt{1 + \omega^2 k_a^2} \tag{12}$$

Now then, based on equation (12), equation (10) becomes:
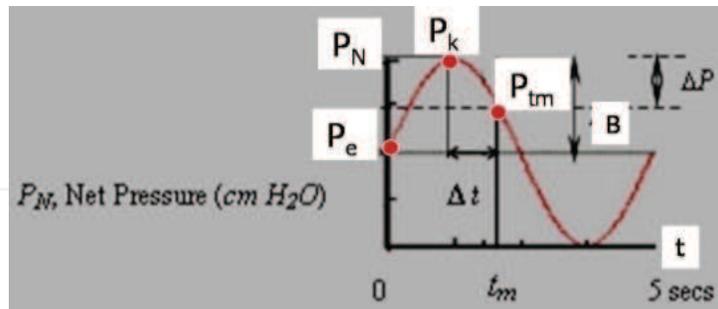
Fig. 26. (reproduced)

$$V(\,t=t_m) = \text{TV} = \frac{BC_a}{\sqrt{1+\omega^2 k_a^2}} \tag{13}$$

**Determining Lung-Compliance (Ca) and Air-Flow Resistance (Ra):**
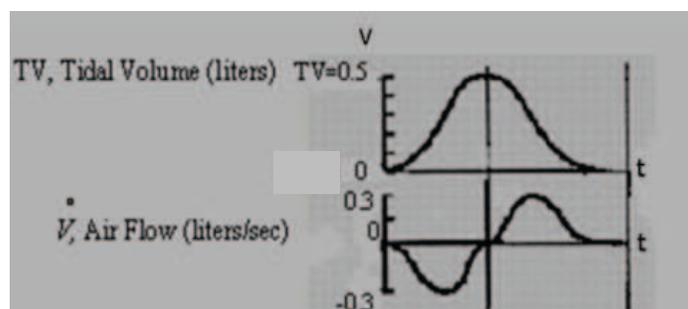
From equations (13 and 7), we get:

$$C_a = \frac{\text{TV}\sqrt{1+\omega^2 k_a^2}}{B} = \frac{\text{TV}}{B\sin\theta} = \frac{\text{TV}(1-\sin\theta)}{\Delta P \sin\theta} \tag{14}$$

Hence, from eqns (7 & 13), the average value of airflow-resistance (R_a) is:

$$R_a = k_a / C_a = \frac{\Delta P \sin\theta (1/\omega\tan\theta)}{\text{TV}(1-\sin\theta)} = \frac{\Delta P \cos\theta}{\text{TV}\omega(1-\sin\theta)} \tag{15}$$

For our patients, the computed ranges of the parameters are:
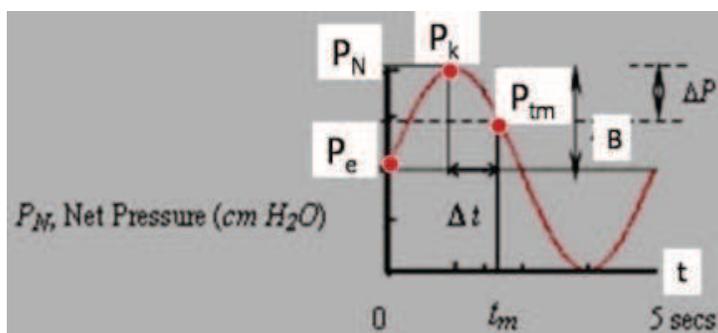
$$C_a = 0.020 - 0.080 \text{ L} / \text{cmH}_2 0 \qquad (16)$$

$$R_a = 9 - 43 \text{ cmH}_2 0 \cdot \text{s} / \text{L}$$

Now, that we have determined the expressions for R_a and C_a, the next step is to develop an integrated index incorporating these parameters.

Formulating a Lung Ventilatory Index (LVI) incorporating Ra and Ca: We now formulate a Lung Ventilatory Index (LVI), incorporating Ra and Ca, as:

$$LVI = \frac{R_a(RF)P_k}{C_a(\text{TV})} \qquad (17)$$

Let us now obtain order-of-magnitude values of *LVI*, for a mechanically ventilated COPD patient in acute respiratory failure:

$$LVI(\textit{Intubated } \text{COPD}) = \frac{[15 cmH_2Os / L][0.33_s{}^{-1}][20 cmH_2O]}{[0.035L / cmH_2O][0.5L]}$$

$$= 5654 \, (cmH_2O / L)^3$$

wherein

$$R_a = 15 \, cmH_2Os / L \qquad C_a = 0.035L / cmH_2O \qquad RF = 0.33_s{}^{-1}$$

$$\text{TV} = 0.5L \qquad P_k = 20 cmH_2O$$

Now, let us obtain an order-of-magnitude of *LVI* (by using representative computed values of R_a, C_a, *RF*, TV, and P_k) as above for a COPD patient with improving lung-status just before successful discontinuation.

$$LVI(\textit{Outpatient } \text{COPD}) = \frac{[10 cmH_2Os / L][0.33_s{}^{-1}][12 cmH_2O]}{[0.05L / cmH_2O][0.35L]}$$

$$= 2263(cmH_2O / L)^3$$

wherein

$$R_a = 10 \, cmH_2Os / L \qquad C_a = 0.050L / cmH_2O \qquad RF = 0.33_s{}^{-1}$$

$$\text{TV} = 0.35L \qquad P_k = 12 cmH_2O$$

Hence, for *LVI* to reflect lung-status improvement in a mechanically ventilated COPD patient in acute respiratory failure, it has to decrease to the range of *LVI* for an outpatient COPD patient at the time of discontinuation.

In fig. 27, it is shown that for the 6 successfully-discontinued cases, the *LVI* was (2900) ± (567) $(cmH_2O/L)^3$; for the 7 failed-discontinuation cases the *LVI* was (11400) ± (1433) $(cmH_2O/L)^3$. It can be also observed that *LVI* enables clear separation between failed and successful discontinuation, which again points to the efficacy of *LVI*.

(6) Successful Extubation Case   (7) Failed Extubation Case
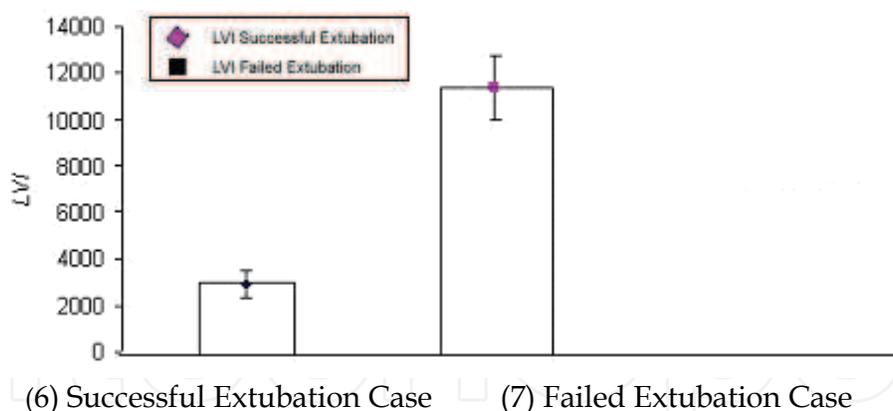
Fig. 27. Distribution of *LVI* at discontinuation for patients with failed and successful discontinuation. For the 6 successfully-discontinued cases, the *LVI* was (2900) ± (567) (cmH_2O/L)^3; for the 7 failed-discontinuation cases the *LVI* was (11400) ± (1433) (cmH_2O/L)^3. It is observed that *LVI* enables clear separation between failed and successful discontinuation [12].

10. Monitoring: Noninvasive determination of aortic pressure, aortic modulus (stiffness) and peripheral resistance)

The aortic blood pressure waveform contains a lot of information on how the LV contraction couples with the aortic compliance and peripheral resistance. Since accurate measurement of aortic blood pressure waveform requires catheterization of the aorta, we have developed a noninvasive method to determine the aortic pressure profile along with the aortic volume-elasticity and peripheral resistance. Fig 28 displays such a constructed aortic pressure profile.

The input to the model consists of auscultatory cuff diastolic and systolic pressures, along with the MRI (or echocardiographically) measured ejection volume-time profile (or volume input into the aorta). The governing differential equation for pressure response to LV outflow rate *I(t)* into the aorta is given by [13]:

$$\frac{dP}{dt} + \lambda P = m_a \left[I(t) + T_a \frac{dI}{dt} \right] \tag{1}$$

where (i) m_a is the aortic volume elasticity *(dP/dV)*, (ii) R_p is the resistance to aortic flow *(=P/Q)*, (iii) $\lambda = m_a/R_p$, (iv) *I(t)* is the monitored inflow rate into the aorta, and (v) T_a is the flow-acceleration period.

This governing equation is solved for measured *I(t)* and *dI/dt* during the systolic phase from time T_1 to T_3 (Fig. 28). For the diastolic-phase solution from time T_3 to T_4, the right-hand side is zero. The solutions for diastolic and systolic phases are given below by equations (2) and (3) respectively.

Solutionequations:

- During diastolic phase,

$$P_d(t) = P_1 e^{\lambda(T-t)} \tag{2}$$

At $T = T_4$, $P_d(T)$=auscultatory P_{ad} =P_1
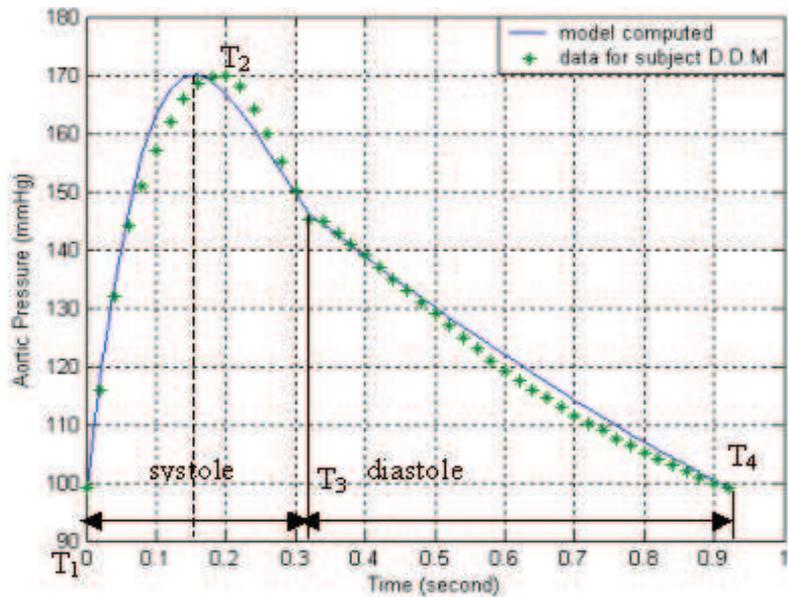
Fig. 28. Model computed cyclic Aortic pressure profile, compared with measured pressure values. The systolic phase from *T1* to *T3* is when blood is ejected into the aorta. The diastolic phase is from *T3* to *T4* [13].

- During systolic phase,

$$P_s(t) = (P_1 - A_1)e^{-\lambda t} + e^{-bt}\left[A_1\cos(\omega t) + A_2\sin(\omega t)\right] \tag{3}$$

where

$$A_1 = \frac{m_a a\omega(T_a\lambda - 1)}{(b - \lambda)^2 + \omega^2}$$

$$A_2 = \frac{m_a a[(\omega^2 + b^2)T_a + \lambda - b - T_a b\lambda]}{(b - \lambda)^2 + \omega^2}$$

Also, as noted in Fig 28, the boundary values are:

At t $=T_2$, $dP_s/dt =0$; at t $=T_2$, $P_s(T_2) = $ auscultatory $P_{as}= P_2$; at t $= T_3$, $P_s(t =T_3) = P_d(t =T_3)$

Hence, based on these boundary values, the following equations are to be solved.

$$\frac{dP_s(t)}{dt}(t = T_2) = -C_1\lambda e^{-\lambda T_2} + e^{-bT_2}\left[A_3\cos(\omega T_2) - A_4\sin(\omega T_2)\right] = 0 \tag{4}$$

- At $t =T_2$, $P_s =P_2$. Hence, from equations (3 & 4), we get:

$$P_s(t = T_2) = P_2 = C_1 e^{-\lambda T_2} + e^{-bT_2}\left[A_1\cos(\omega T_2) + A_2\sin(\omega T_2)\right] \tag{5}$$

- At $t =T_3$, $P_s(t =T_3) = P_d(t =T_3)$. Hence, from equations (2 and 3), we obtain:

$$P_1 e^{\lambda(T-T_3)} = (P_1 - A_1)e^{-\lambda T_3} + e^{-bT_3}\left[A_1\cos(\omega T_3) + A_2\sin(\omega T_3)\right] \tag{6}$$

We now solve equations (4, 5 & 6), to determine the unknown parameters m_a, R_p (and T_2).

We have determined the expressions for the aortic pressure during the systolic and diastolic phases, by solving the governing equation (1), for the monitored LV outflow rate (or input into the aorta) $I(t)$, using (i) the monitored auscultatory diastolic pressures (P_{ad}), to serve as the boundary condition at the beginning of the systolic-phase solution (at time T_1) and at the end of the diastolic-phase solution (at time T_4), (ii) the monitored auscultatory systolic pressure (P_{as} =P_2) to represent the maximum value of the systolic-phase solution.

Because the pressure solution of equation (1) is a function of m_a and R_p, we first determine the values of these parameters by making the solution satisfy the above-mentioned boundary conditions, which in turn yields the pressure profile given by $P_d(t)$ and $P_s(t)$. This non-invasively determinable aortic pressure can provide hitherto unavailable information on vascular compliance and resistance status, as well as on the capacity of the LV to respond to it.
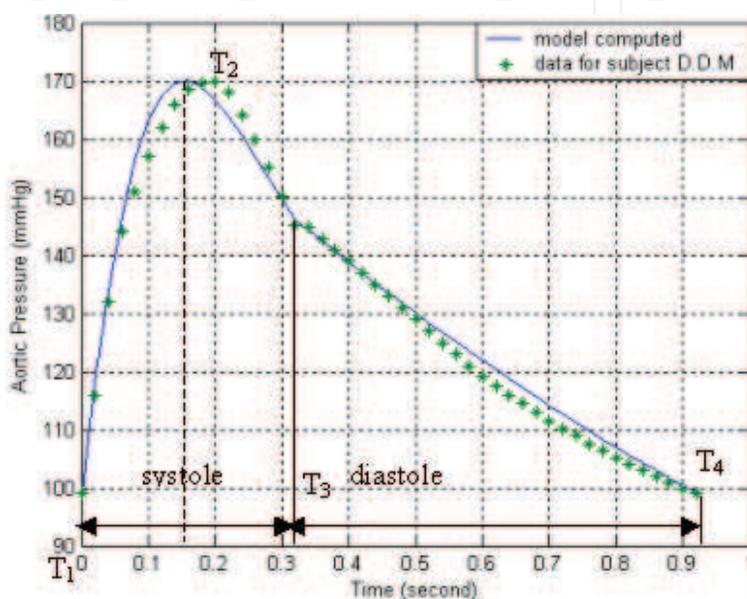

Fig. 29. Plot of aortic pressure (of patient B) during one cardiac cycle, t_e=0.32s. Herein, T_1-T_3 represents the systolic phase, and T_3-T_4(=0.92s) represents the diastolic phase. At T_2, the aortic systolic pressure profile has its maximal value (=P_s). The scatter points are the data measured from catheterization. The solid line is the model-computed profile; RMS=2.41 mmHg. Note the excellent correlation between the model-derived aortic pressure profile and the catheter-obtained aortic pressure profile.

In **Fig. 29**, the model-computed aortic pressure profile patient B (with double vessel disease and hypertension) is shown, along with the actual catheter pressure data. We can note how well the model-computed result matches the actual catheterization data, with RMS 2.41 mmHg. The aortic stiffness (m_a) and peripheral resistance (R_p) are obtained to be 1.03 *mmHg/ml* and 1.59 *mmHg·s/ml*, respectively.

Let us consider yet another benefit of this analysis. We have determined aortic pressure profile, aortic stiffness (m_a) or aortic elastance (E_{ao}) and peripheral resistance. From the instantaneous aortic pressure and aortic inflow rate, we can determine the instantaneous left ventricular (LV) systolic pressure, in terms of the instantaneous dimensions of the LV outflow tract. We hence determine the LV systolic pressure profile, from which we can evaluate the traditional contractility index (*dP/dt max*) as well as the LV systolic elastance (*Elv*).

We can then determine the ratio of *Elv/Eao*, to represent the LV-Aorta Matching Index (*VAMI*). In ischemic cardiomyopathy patients, this *VAMI* value is depressed. However, following surgical vascular restoration, this index value is partially restored.

11. Coronary Bypass surgery: Candidacy

- **Interventional candidacy based on computed intra-LV flow-velocity and pressure-gradient distributions**
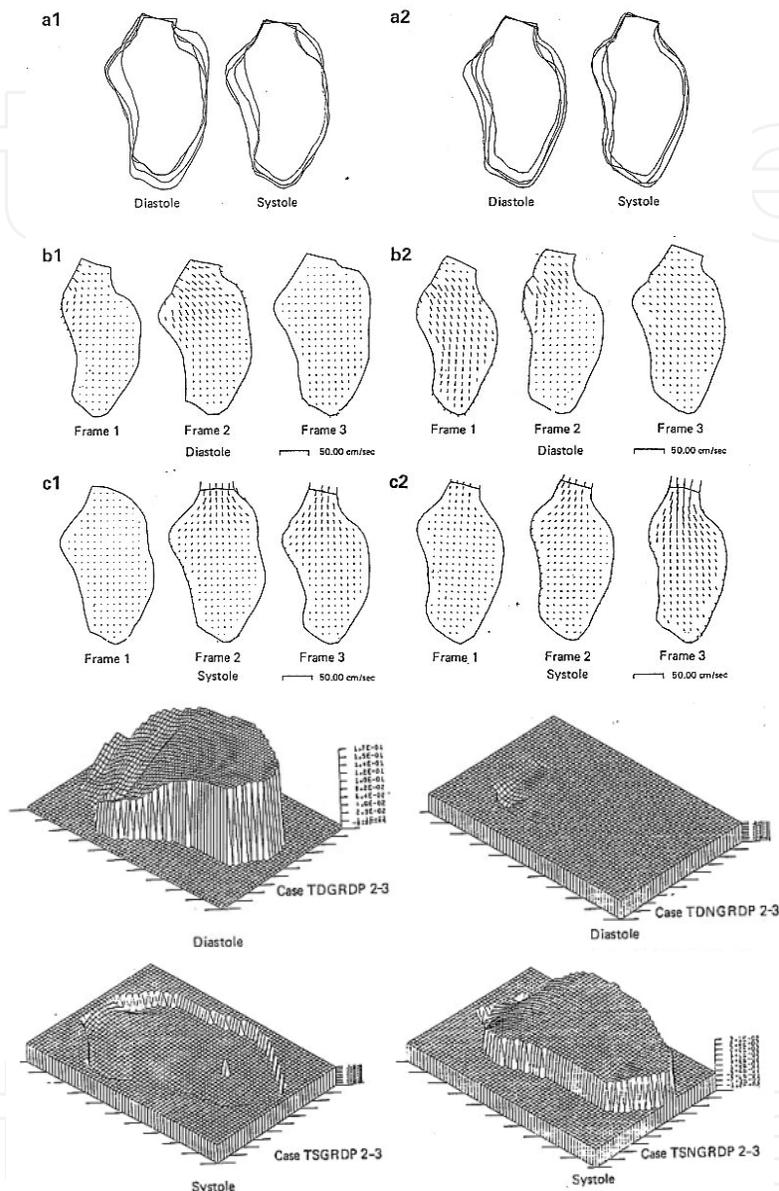

Fig. 30. Construction of Intra-LV Blood flow velocity and pressure-gradient distributions for a patient with myocardial infarct: (a) Superimposed sequential diastolic and systolic endocardial frames (whose aortic valves centers and the long axis are matched), before (1) and after (2) administration of nitroglycerin; (b) Instantaneous intra-LV distributions of velocity during diastole, before (1) and after (2) administration of nitroglycerin; (c) Instantaneous intra-LV distributions of velocity during ejection phase, before (1) and after (2) administration of nitroglycerin, (d) Instantaneous intra-LV distributions of pressure-differentials during diastole, before (1) and after (2) administration of nitroglycerin; (e) Instantaneous intra-LV distributions of pressure-differential during ejection phase, before (1) and after (2) administration of nitroglycerin. (Adapted from reference 14: Subbaraj K, Ghista DN, Fallen EL, *J Biomed Eng* 1987, 9:206-215.).

A left ventricle with ischemic and infarcted myocardial segments will have lowered ejection fraction and cardiac output, because it will not be able to generate adequate myocardial contraction to raise the intra-LV pressure above aortic pressure for a ling enough duration to generate adequate stroke volume. These patients need coronary bypass surgery, and a pre-surgical assessment of their candidacy for it, on how much they can from it. For this purpose, we need to determine the intra-LV blood flow velocity and pressure-gradient profiles before and after the administration of nitroglycerin.

So, we carry out a CFD analysis of intra-LV blood flow. The data required for the CFD analysis consists of: LV 2-D long-axis frames during LV diastolic and systolic phases; LV pressure vs. time associated with these LV frames; Computation of LV instantaneous wall velocities as well as instantaneous velocity of blood entering the LV during the filling phase and leaving the LV during the ejection phase.

From this CFD, we have determined the instantaneous distributions of intra-LV blood-flow velocity and differential-pressure during filling and ejection phases, to intrinsically characterize LV resistance-to-filling (LV-RFT) and contractility (LV-CONT) respectively. The results are summarized in the above Fig. 30.

By comparing intra-LV pressure-gradients before and after administration of nitroglycerin (a myocardial perfusing agent, and hence a quasi-simulator of coronary bypass surgery), we can infer how the myocardium is going to respond and how these LV functional indices will improve after coronary by bypass surgery.

12. Theory of hospital administration: Formulation of hospital units' performance index and cost-effective index

A Hospital has clinical services departments, medical supply and hospital-services departments, financial-management and administrative departments. Each of these five sets of departments has to function in a cost-effective fashion.

Let us, for example, consider the Intensive-Care Unit (ICU) department. The human resource to an ICU dept consists of physicians and nurses. Using activity-based costing, we can determine the human-resource strength, based on an assumed reasonable probability-of-occurrence of (for instance) two patients simultaneously (instead of just one patient) having life-threatening episodes.

Performance Index: We can formulate the ICU performance-indicator in terms of the amounts by which the physiological health-index (PHI or NDPI) values of patients were (i) enhanced in the ICU for those patients discharged into the ward from the ICU, and (ii) diminished in the ICU in the case of patients who died in the ICU.

Let us say that patients are admitted to the CCU if their Physiological-health-index (PHI) value falls below 50%. So if the PHI of a patient improves from 30 to 50, then the **Patient-HealthImprovement Index (PHII)** for that patient is given by [15],

$$\text{PHII} = \left(\frac{50-30}{30}\right) 100 = 67 \ (or \ 67\%) \tag{1}$$

Thus the **patient health-improvement index (PHII)** value is higher if a more seriously-ill patient is discharged from the ICU, and lower if a not-so-seriously ill patient is discharged, i.e., if

$$\text{PHII} = \left(\frac{50-40}{40}\right) 100 = 25 \ (or \ 25\%) \tag{2}$$

We can then formulate the **Performance-index (PFI)** for an ICU as follows:

$$ICU \text{ Performance index (PFI)} = \frac{\sum PHII \text{ of the patients}}{\text{\# of those patients treated during a life time period}} \quad (3)$$

Hence, the higher the value of ICU performance index, the better is the performance of the ICU. If now a patient dies, as a result of the PHII becoming negative (i.e slipping from (say) 30 to 10), then

$$PHII = 100 \left(\frac{10 - 30}{30} \right) = -67 \quad (4)$$

As a result, ΣPHII (in equation 3) will decrease, and the overall value of ICU performance index (namely PFI, as calculated by means of eq. 3), will fall.

Cost-Effective Index: Now, let us consider that (i) we have one physician and five nurses for a 10 bed CCU, based on the probability-of-occurrence of two patients having life-threatening events being say 0.2 (or 20%), and that (ii) for this human resource/staffing, the ICU performance index value (PFI) is (say) 40.

If we increase the staffing, the ICU performance index value could go upto 50 or so, at the expense of more salary cost. So now we can come up with another indicator namely, **Cost-effectiveness index (CEI)**

$$CEI = \frac{\text{Performance index}}{\text{Total salary index (in salary - units)}}$$

$$= \frac{\text{Performance index}}{\text{Resource index (in terms of salary - units)}} \quad (5)$$

wherein, say, a salary of 1000=0.1 unit, 10,000=1 unit, 20,000=2 units, and so on.

So if an ICU has one physician with a monthly salary of 20,000 (i.e. 2 salary-units) and four nurses each with a total monthly salary of 5,000 (i.e. total of 2.0 salary-units), then

$$\textbf{CEI}(ICU) = \frac{\text{Performance index (of 40)}}{\text{Salary-units Index or Resource Index}, R_i \, [= (2 + 2.0)]}$$

$$= \frac{40}{4.0} = 10 \quad (6)$$

Now, let us assume that we raise the **PFI** (ICU) to (say) 60 by augmenting the nursing staff, so as to have six nurses (R_i = 3 units) and 1.5 full-time equivalent physician-on-duty (R_i = 3 units), then

$$CEI \ (ICU) = \frac{PFI}{R_i} = \frac{50}{(3 + 3)} = 8.3 \quad (7)$$

So while the PFI of ICU has gone up from 40 to 50, the CEI of ICU has gone down from 10 to 8.3.

Strategy of Operation: Our strategy would be to operate this Performance-Resource system, in such a way that we can determine the resource index R_i for which we can obtain acceptable values of both PFI and CEI. In a way, figure (31) could represent this balance between PFI & CEI, in order to determine optimal Resource Index or resource [15].

With reference to this **figure 31**, if we have a resource value of $R_i = R_1$, then the corresponding PFI (=PFI_1) will be unacceptable, as being too low; hence, we will want to increase the value of R_i. If we have a resource value of $R_i = R_2$, then our corresponding CEI (= CEI_2) will also be unacceptable, for being too low; hence we will want to decrease R_i. In doing so, we can arrive at the optimal value R_{io}, for which both CEI and PFI are acceptable. This procedure, for converging to $R_i = R_{i0}$, can be formulated computationally.
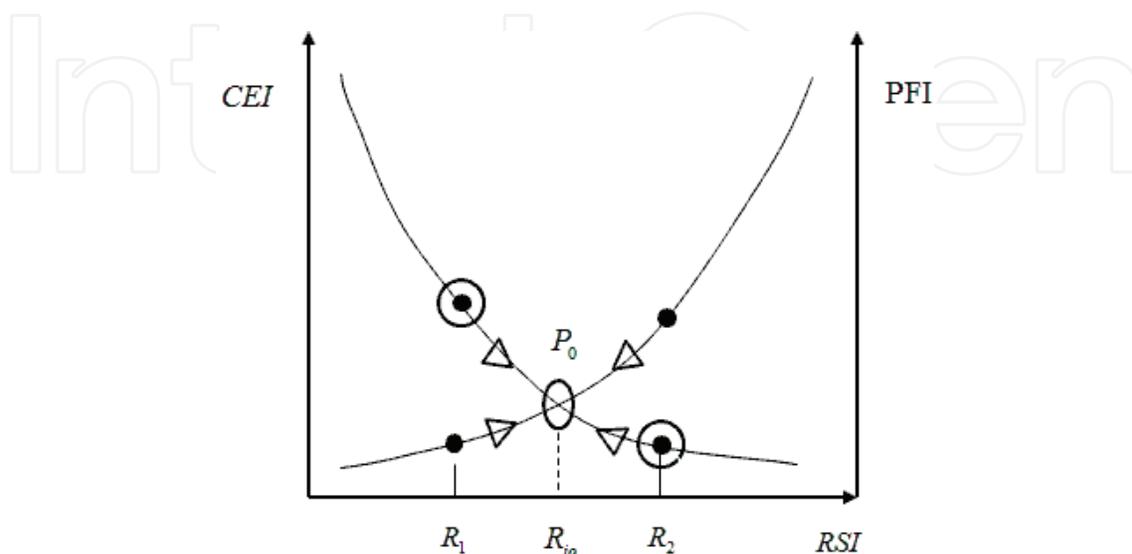
Fig. 31. Optimising the value of R_i so to obtain acceptable values of CEI and PFI [15].

Now then, let us formulate how a hospital budget can be optimally distributed. Let us say that a Hospital has 'n' number of departments and a prescribed budget (or budget index, BGI). We would want to distribute the budget among the departments, such that none of the 'n' departments has a PFI below the acceptable value of PFI_a and a CEI below the acceptable value of CEI_a**.**

So the Operational research problem is to be formulated as follows:

How to distribute or divide the given Budget (or Budget Index Value) into R_i (i= 1,……..,n), such that $PFI_i \geq PFI_a$, for all i; and $CEI_i \geq CEI_a$, for all i This then is the prime task of a Hospital administrator!

Summarizing:

The ICU Operational cost (OPC) is the cost of operating the ICU over this one month period. The ratio of this ICU PFI and the ICU OPC is the Cost-effectiveness index (CEI) of ICU.
The Management strategy is to maintain certain acceptable values of both PFI and CEI for all hospital departments, by judicious allocation of staff to the departments.
This enables the determination of optimal Resource index (RSI) and hospital budget (HOB) to maintain a balance between PFI and CEI for all the hospital departments. This can constitute the basis of Hospital Management.

13. *How to proceed*: For biomedical engineering to become a professional field

So in this chapter, we have talked about:
1. *Anatomy:* Spine as an optimal structure,
2. *Physiology:* Mechanism of LV pressure generation

3. Non-dimensional Physiological Index
4. *Medical Test:* Cardiac Fitness based on Treadmill Heart Rate Variation
5. *Medical Physiology:* A Non-dimensional Diabetes Index with respect to Oral-Glucose-tolerance Testing
6. *Cardiology:* LV Contractility based on its normalized wall stress
7. *Diagnostics:* LV Contractility based on its shape factor
8. *ICU Evaluation:* Indicator for lung-status in Mechanically ventilated Copd patients, using lung ventilation modeling and assessment
9. *Monitoring:* Noninvasive determination of Aortic pressure, aortic stiffness and peripheral resistance
10. *Coronary Bypass Surgery:* candidacy
11. Hospital Operations Management

We have shown how biomedical engineering (BME) can open up a new approach to the study of Anatomy, in terms of how anatomical structures are intrinsically designed as optimal structures for their function.

We have also seen how BME can be applied to the study of Physiology, by modelling of physiological systems (as bme models), which can enable us to assess their performance for clinical usage by means of our novel NDPIs comprised of the physiological systems' model parameters. The NDPIs can considerably facilitate medical assessment, and lead us to what can be effectively termed as Higher-order Translational Medicine (HOTM), entailing the incorporation of physical and engineering sciences into medical sciences and clinical sciences for more reliable and effective patient care.

Even Medical tests can be adroitly modelled as BME systems. These systems are formulated in the form of mathematical models, whose solutions are simulated to the medical tests data, to evaluate the model parameters. The model parameters can be combined into NDPIs, by means of which the test data can be analysed for making more reliable medical assessment and decisions.

Finally, we have seen how we can bring to bear the enormous scope of Industrial Engineering (and constrained optimisation theory) to hospital operational management, so as to develop (i) cost-effective performance indices of hospital departments, and (ii) more knowledgeable framework for budget development and allocation to the various department.

Putting all of this together is what will justify (i) the incorporation of BME into the MD curriculum, and (ii) its constituting an indispensable patient-care oriented department in tertiary- care hospitals.

This verily constitutes the biomedical engineering professional trail, from anatomy and physiology to medicine and into hospital administration. This is what the professional role of biomedical engineering needs to be, to promote a higher order of translational medicine and patient care.

14. References

[1] Nondimensional Physiological Indices for Medical assessment, by Dhanjoo N. Ghista, in *J of Mechanics in Medicine and Biology*, Vol 9, No 4, 2009.

[2] *Applied Biomedical Engineering Mechanics*, by Dhanjoo N. Ghista, CRC press (Taylor & Francis Group) Baton Rouge Florida 334872-2742, ISNBN 978-0-8247-5831-8,2008

[3] Human Lumbar Vertebral Body as an Intrinsic Functionally-optimal Structure, by D.N. Ghista, S.C. Fan, K.Ramakrishna, I.Sridhar, in *International Journal of Design and Nature*, 2006, 1(1): 34-47.

[4] The Optimal Structural design of the human Spinal Intervertebral disc", by D.N.Ghista, S.C.Fan, I.Sridhar, K.Ramakrishna, in *International Journal of Design and Nature*, 2006, 1(2).

[5] Mechanism of Left Ventricular Pressure increase during Isovolumic contraction, and determination of its Equivalent myocardial fibers orientation, by Ghista, DN, Liu Li, Chua LP, Zhong L, Tan RS, Tan YS; in *J Mech Med Biol*, 2009, 9 (2), 177–198

[6] Cardiac Fitness mathematical Model of Heart-rate response to V02 during and after Stress-Testing", Lim GeokHian, Dhanjoo N. Ghista, Koo TseYoong, John Tan Cher Chat, Philip EngTiew& Loo Chian Min; *International Journal of Computer Application in Technology(Biomedical Engineering & Computing Special Issue),* Vol 21, No 1/2, 2004.

[7] Glucose Tolerance Test Modeling & Patient-Simulation for Diagnosis, by Sarma Dittakavi & Dhanjoo N. Ghista, *Journal of Mechanics in Medicine & Biology,* Vol. 1, No.2, Oct.2001.

[8] Clinical Simulation of OGTT Glucose Response Model for Diagnosis of Diabetic Patient, by Dhanjoo N.Ghista, Patrick S.K. Chua, Andy UtamaAulia, Peter L.P. Yeo, in *Journal ofMechanics in Medicine & Biology* 2005 Vol 5, No. 1.

[9] Validation of a novel noninvasive characterization of cardiac index of left ventricle contractility in patients, by Zhong L, Tan RS, Ghista DN, Ng E. Y-K, Chua LP, Kassab GS, *Am J Physiol Heart CircPhysiol*2007, 292:H2764-2772.

[10] LV shape-based contractility indices, by Liang Zhong, Dhanjoo N. Ghista, Eddie Y-K. Ng, Lim SooTeik and Chua Siang Jin, CN Lee, in *Journal of Biomechanics*, 2006, 39: 2397-2409.

[11] Measures and Indices for Intrinsic Characterization of Cardiac Dysfunction during Filling and Systolic Ejection, by Liang Zhong, Dhanjoo N. Ghista, Eddie Y. Ng, Lim SooTeik, and Chua Siang Jin, in *Journal of Mechanics in Medicine and Biology*,Vol 5, No. 2, 2005.

[12] Indicator for Lung-status in a mechanically Ventilated (COPD) Patient using Lung Ventilation Modeling and Assessment, by D.N.Ghista, R. Pasam, S.B. Vasudev, P.Bandi, and R.V. kumar in *Human Respiration Anatomy and Physiology, Mathematical Modellings and Applications*, ed by Vladimir Kulish, WIT Press, 2006.

[13] Determination of Aortic Pressure-time Profile, Along with Aortic Stiffness and Peripheral Resistance, by Liang Zhong, Dhanjoo N. Ghista, Eddie Y-K. Ng, Lim SooTeik and Chua Siang Jin, in *Journal of Mechanics in Medicine & Biology* 2004, 4(4):499-509.

[14] Intrinsic Indices of the Left Ventricle as a Blood Pump in Normal and Infarcted Left Ventricle, by K. Subbaraj, D.N. Ghista, and E. L. Fallen, in *J of Biomedical Engineering*, Vol 9, July issue, 1987

[15] Physiological Systems' Numbers in Medical Diagnosis and Hosipital Cost-effective Operation, by Dhanjoo N. Ghista, in *Journal of Mechanics in Medicine & Biology* 2005, vol 4, No.4.
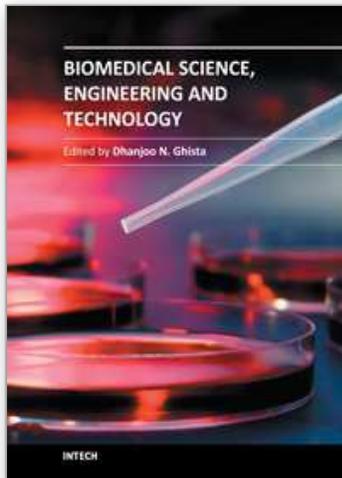
Biomedical Science, Engineering and Technology

Edited by Prof. Dhanjoo N. Ghista

This innovative book integrates the disciplines of biomedical science, biomedical engineering, biotechnology, physiological engineering, and hospital management technology. Herein, Biomedical science covers topics on disease pathways, models and treatment mechanisms, and the roles of red palm oil and phytomedicinal plants in reducing HIV and diabetes complications by enhancing antioxidant activity. Biomedical engineering coves topics of biomaterials (biodegradable polymers and magnetic nanomaterials), coronary stents, contact lenses, modelling of flows through tubes of varying cross-section, heart rate variability analysis of diabetic neuropathy, and EEG analysis in brain function assessment. Biotechnology covers the topics of hydrophobic interaction chromatography, protein scaffolds engineering, liposomes for construction of vaccines, induced pluripotent stem cells to fix genetic diseases by regenerative approaches, polymeric drug conjugates for improving the efficacy of anticancer drugs, and genetic modification of animals for agricultural use. Physiological engineering deals with mathematical modelling of physiological (cardiac, lung ventilation, glucose regulation) systems and formulation of indices for medical assessment (such as cardiac contractility, lung disease status, and diabetes risk). Finally, Hospital management science and technology involves the application of both biomedical engineering and industrial engineering for cost-effective operation of a hospital.

INTECH
open science | open minds

www.intechopen.com

Fax: +385 (51) 686 166
www.intechopen.com

Fax: +86-21-62489821